University of Durham

Modelling Oscillatory Behaviour of Elastic Rods with Variable Structure

Department of Mathematical Sciences

Alexander ROWAN-SMITH

Supervised by Dr. Christopher PRIOR

April 30, 2021

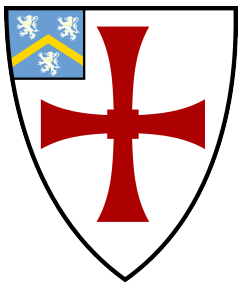

Declaration

This piece of work is a result of my own work except where it forms an assessment based on group project work. In the case of a group project, the work has been prepared in collaboration with other members of the group. Material from the work of others not involved in the project has been acknowledged and quotations and paraphrases suitably indicated.

Acknowledgements

I would personally like to express my gratitude to my supervisor Dr Chris Prior for providing me the opportunity to work on such a fascinating project. Finally, I would like to acknowledge all the continued support my friends and family have given throughout the project and beyond.

Abstract

Until the turn of the century, research into a varied internal structure of elastic rods had been sparse. Whilst models of Kirchhoff rods in an equilibrium state have been frequently documented, transferring to a more precise, time-dependent dynamical system introduces a higher degree of complexity. However, the combination of these two factors has rarely been studied and reported upon.

Modifying the profile of the flexural rigidity accounts for the shift in behaviours of rods with non-uniform structure. By relating this to a perceived thickness, this concept could be mathematically modelled, producing simulations of numerous rods with varying physical shape. With the aim to categorise distinguished solutions, I move to observe simulations representing real-world instances, giving reasoning for the types of behaviour shown according to its specific purpose.

Table of Contents

List of Figures

The animations in these figures are viewable inline when this paper is opened in Adobe Acrobat Reader.

Section 1

Introduction

Applications of an elastic rod model span a wide variety of disciplines. From macroscopic engineering to microscopic biology, I aim to expand on the initial research done by Kirchhoff and Clebsch circa 1860 [1, 2], to create a generalised rod model that is accountable for variations in diameter. The idea of this model was first proposed by Jacob Bernoulli in 1691, then solved by Leonhard Euler in 1744 (both cited in Matsutani, 2010) [3] to give a new branch of mathematics, known as the *elastica theory*.

1.1 Project Motivation

In general, the elastica theory describes a slender-bodied rod with elastic properties having one dimension vastly larger than any other. Bending, torsion and stretching can all be modelled by the changing in curvature of a centerline. In reality, these types of rods occur both in nature and man-made objects such as undersea cables; though more interestingly, it is the function of naturally occurring rods that partially define their own structure.

Throughout the last few decades, more research into the area has become apparent. Investigation into the case where forces exist[(1)], however, often assume that the bending stiffness of the system remains constant as a simplicity. In many real-world cases this is in fact imprecise, where the inclusion of a varied bending stiffness can alter the solution of the model by a relatively considerable degree. Also referred to as the *flexural rigidity*, and used interchangeably, the bending stiffness is a material property measuring the resistance to deformation under stress. I, therefore, move to investigate how the changing of both

(1) Known as the dynamical case.

internal and external structures affect the behaviour of elastic rods, with an emphasis on demonstrating the magnitude of deviation from cases making this constant assumption.

1.2 Pre-existing Mathematical Research

Kirchhoff initially aimed to convey his theory in terms of the variational theorem, whereas Clebsch dissected the rod into segments, implying each segment was subject to a force (as cited by Dill, 1992) [4]. Nearing the end of the nineteenth century, Augustus Love intended to prove the equations of Kirchhoff-Clebsch in an entirely different manner, as portrayed by Truesdell in Dill's 'Kirchhoff's theory of rods' [4]:

> "*He* [Love] *took the modern global point of view and assumed that the deformed state differs by small deformations from a motion in which cross sections remain plane, undistorted, and normal to the axis.*"
>
> — Truesdell, C. (1992)

A mathematical model of the elastica theory can be applied to various cases due to its robustness; because of this, the theory has been developed and improved upon since its construction in the early eighteenth century. Only the equilibrium case was initially considered, but the continued research from Kirchhoff and Clebsch published in 1859 and 1862 respectively, sparked a delayed interest into the dynamical, time-dependent case by the twentieth century.

Perhaps triggered as a result of the surge of modern medicine, in the twentieth century, the dynamical case became more prevalent and had biological applications in the modelling of deoxyribonucleic acid (DNA), bacterium and flagella. In fact, Goyal, Perkins and Lee (2005) investigated the quasi-static, dynamical case of modelling DNA and three-dimensional supercoils in their published work, titled: 'Nonlinear dynamics and loop formation in Kirchhoff rods with implications to the mechanics of DNA and cables' [5].

The introduction of a variable bending stiffness is non-trivial, so is often used in conjunction with the equilibrium case for simplicity. Nevertheless, as an example, flagella should not be accurately modelled using a constant bending stiffness; that is the whipping motion often seen in flagella occurs as a consequence to its non-uniform structure. Dias and Audoly (2015) began to introduce the concept of a variable width within ribbons, citing and extending Wunderlich's and Sadowksky's models in the case of equilibrium [6], where, three years later, Silverman and Farrah (2018) [7] investigated the variation in geometry of a tapered cantilever. However, there is no obvious published work investigating variable

structures within the dynamical case, particularly in the non-quasi-static instance.

1.3 Establishing an Original Approach

The overarching intention, therefore, is to expand on all pre-existing mathematical research to manufacture a model, incorporating a dynamical Kirchhoff rod with variable structure. The reason for this is to create a model that develops throughout time.

The way in which I plan to introduce this is through a linear relationship with the bending stiffness, suggesting that this is proportional to some radial function defining thickness across its profile, along with a non-uniform material density.

For situations with only small perturbations in geometry, the system may be solved precisely, or even analytically using methods from the variational theorem. Yet, for most situations in our specific case, this may not always be true. Therefore, I shall also employ several numerical methods such as the fourth order Runge-Kutta (cited in Weiss, 2002) and Adams-Bashforth methods, to obtain approximate, but accurate, solutions to our model [8]. Even so, it is a known problem that certain solutions will inevitably become unstable as a result of bifurcation conditions[(2)] (Goyal, Perkins and Lee, 2005) [5].

1.4 Project Scope

With a formulated model, I look ahead and anticipate certain families of solutions based on the variation of width, with a purpose to categorise them based on observed behaviour. The idea of this model is to simulate more accurate solutions of the rod, so I therefore also aim to demonstrate the benefits of this model and justify my reasoning for making this modification of the dynamical Kirchhoff system.

As with all branches of mathematics, the theory endeavours to describe, and in particular here, material objects. Consider this, I look to apply the model to real-world examples and compare the behaviours to already categorised solutions, giving insight into possible explanations for the structure's profile, based on functionality.

(2) Defined in the glossary, the bifurcation theory is the study of variations in solutions of dynamical systems.

Section 2

Model Formulation

To describe the system I plan to work with, classical mechanics are used to introduce formulae to begin to develop the system mathematically. The model will simply contain an isolated object, namely the elastic rod, where the rod's position can modelled, whilst experiencing external forces, as a function of time. By also incorporating internal forces, the aim is to model the variation in geometry of a rod subjected to these forces, in two-dimensional space at a large quantity of generalised points over time. The following derivation is an adaptation of the model by Prior (2020) [9].

2.1 Space Curve Geometry

Under such forces, one can investigate the change in profile of the rod's geometry. By making the safe assumption that the entire behaviour is governed by a central curve, the alteration in geometry can be calculated explicitly.

By first mathematically describing the system as a smooth, unit speed space curve $\mathbf{r}(s,t) : [0,L] \times [0,t] \to \mathbb{R}^3 \times \mathbb{R}$, where for a parameterising arc length $s \in [0,L]$, the central curve $\mathbf{r}(s,t)$ maps to a point in three-dimensional space at a given time t. Dependent on time, this centre-line $\mathbf{r}$ moves throughout the domain and will change geometry under some experienced forces.

Having characterised a space curve, a basis for all s along the curve of length L assists in modelling the effects experienced by the rod and can be defined by differential geometry in the following way.

Definition.

For $\mathbf{r} : I \to \mathbb{R}^3$ a smooth unit speed space curve in some interval I, $\mathbf{t}(s) = \mathbf{r}'(s)$ is its *tangent vector*[3] and, moreover, the *curvature of* $\mathbf{r}$ is defined as,

$$\kappa(s) \coloneqq \left\|\mathbf{t}'(s)\right\| = \left\|\mathbf{r}''(s)\right\|.$$

Then, for κ non-zero, $\mathbf{n}(s) = \frac{1}{\kappa(s)} \cdot \mathbf{t}'(s)$ exists and is the *principal normal vector* to the curve $\mathbf{r}(s)$. To complete the basis, the vector orthogonal to both $\mathbf{n}(s)$ and $\mathbf{t}(s)$ is $\mathbf{b}(s) \coloneqq \mathbf{t}(s) \times \mathbf{n}(s) \in \mathbb{R}^3$, which is the *binomial vector of* $\mathbf{r}$. Combining these vectors, the oriented orthonormal basis $\left[\mathbf{t}(s), \mathbf{n}(s), \mathbf{b}(s)\right]$ is called the *moving frame basis*[4]. The *torsion of* $\mathbf{r}$ at a point s is defined by,

$$\mathbf{b}'(s) = \tau(s)\mathbf{n}(s).$$

Conjecture. (Frenet-Serret Formulae)

Given $\mathbf{r}(s)$ and its corresponding moving frame, then for $\kappa \neq 0$ the following relations can be proved,

$$\begin{aligned} \mathbf{t}'(s) &= \kappa(s)\mathbf{n}(s), \\ \mathbf{n}'(s) &= \tau(s)\mathbf{b}(s) - \kappa(s)\mathbf{t}(s), \\ \mathbf{b}'(s) &= \tau(s)\mathbf{n}(s). \end{aligned} \tag{2.1}$$

Taking the basis, I relabel it to the orthonormal triad $(\mathbf{d}_1, \mathbf{d}_2, \mathbf{d}_3)$, where $\mathbf{d}_3 = \mathbf{t}(s)$. Now considering any twisting and bending of the rod, the curve is restricted to the plane spanned by the vectors $\mathbf{d}_1$ and $\mathbf{d}_2$, which are linearly independent of each other. Therefore, any twisting that occurs happens solely in the $\mathbf{d}_3$, tangent, direction. Figure (2.1) shows two examples of rods, given a central curve $\mathbf{r}$ and a visual representation of the moving frame basis used at every point s along its entire profile.

---

(3) This vector is inherently unit by the properties of unit speed curves.

(4) This frame is also known as the *Frenet-Serret basis.*

(5) Given any space curve $\mathbf{r}(s)$, the equation of the tubular surface at a radius r_0 from the curve is $S(s, \theta) \coloneqq \mathbf{r}(s) + r_0\left[\mathbf{b}(s)\sin\theta\text{-}\mathbf{n}(s)\cos\theta\right]$, as in Figures (2.1a) and (2.1b).

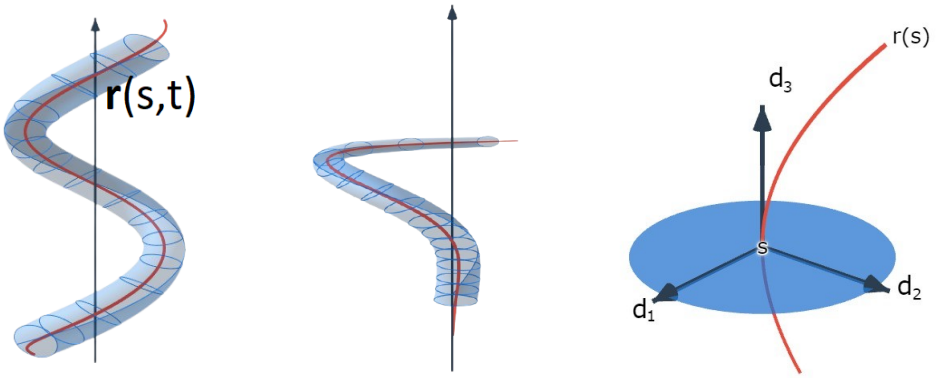

(a) (b) (c)

Figure 2.1: (a), (b): Visual representation of two different curves $\mathbf{r}$ in Euclidean space, with tubes around the curves, showing the thickness of rods with small radii. (c) Visual representation of the Frenet-Serret basis in three dimensions.[5]

2.2 Mechanical Twisting and Curvature

Under any force or moment, one would expect the rod's profile to deform; this is represented by moments of twisting and bending. In a geometrical sense, a tensor is required that acts on the basis, causing it to move and rotate in three-dimensional space.

Let $u_1(s)$, $u_2(s)$ be functions illustrating the rate of bending in the directions $\mathbf{d}_1$ and $\mathbf{d}_2$ respectively, along with $u_3(s)$ the rate of twisting. Then a combined rotation tensor Ω is defined as,

$$\Omega \coloneqq u_1\mathbf{d}_1 + u_2\mathbf{d}_2 + u_3\mathbf{d}_3, \tag{2.2}$$

such that,

$$\frac{d}{ds}\begin{pmatrix}\mathbf{d}_1\\ \mathbf{d}_2\\ \mathbf{d}_3\end{pmatrix} = \begin{pmatrix}0 & u_3 & -u_2\\ -u_3 & 0 & u_1\\ u_2 & -u_1 & 0\end{pmatrix}\begin{pmatrix}\mathbf{d}_1\\ \mathbf{d}_2\\ \mathbf{d}_3\end{pmatrix}. \tag{2.3}$$

Making the assumption that the curve can be restricted to a two-dimensional plane without twisting, that is $u_3 = 0$, it is possible to set either u_2 or u_1 to zero since the axis is planar. Without any loss of generality, I then fix $u_1 = 0$, to explicitly obtain the following:

$$\frac{d}{ds}\mathbf{d}_1 = -u_2\mathbf{d}_3\ ,\ \frac{d}{ds}\mathbf{d}_2 = 0\ ,\ \frac{d}{ds}\mathbf{d}_3 = u_2\mathbf{d}_1, \tag{2.4}$$

$$\frac{d^2}{ds^2}\mathbf{d}_1 = -\frac{du_2}{ds}\mathbf{d}_3 - {u_2}^2\mathbf{d}_1, \tag{2.5}$$

$$\frac{d^2}{ds^2}\mathbf{d}_1 - \frac{1}{u_2}\frac{du_2}{ds}\frac{d}{ds}\mathbf{d}_1 + {u_2}^2\mathbf{d}_1 = 0. \tag{2.6}$$

In terms of $\mathbf{d}_1$, this is a second-order linear differential equation with constant coefficients; hence, for u_2 constant,

$$\mathbf{d}_1 = \sin(u_2 s)\mathbf{d}_3(0) + \cos(u_2 s)\mathbf{d}_1(0). \tag{2.7}$$

By the first equation of (2.4),

$$\mathbf{d}_3 = -\cos(u_2 s)\mathbf{d}_3(0) + \sin(u_2 s)\mathbf{d}_1(0). \tag{2.8}$$

However, with a planar rod[6], one can always write the basis vectors in terms of an angle $\theta(s)$. That is,

$$\mathbf{d}_3 = \big(\cos\theta(s), \sin\theta(s), 0\big)\,,\ \ \mathbf{d}_1 = \big(-\sin\theta(s), \cos\theta(s), 0\big)\,,\ \ \mathbf{d}_2 = (0,0,1)\,. \tag{2.9}$$

From my definitions, $\mathbf{d}_3$ was the unit tangential vector[7],

$$\mathbf{d}_3 = \mathbf{t}(s) = \frac{d\mathbf{r}(s)}{ds}, \tag{2.10}$$

which can, in turn, be solved for $\mathbf{r}(s)$, as the anti-derivative of $\mathbf{d}_3$ with fixed initial position $\mathbf{r}_0$,

$$\mathbf{r}(s) = \mathbf{r}_0 + \int_0^s \big(\cos\theta(s'), \sin\theta(s'), 0\big)\ \mathrm{d}s'. \tag{2.11}$$

2.3 Internal and External Forces

Having described the geometry of the system quantitatively, I look to a rod subjected to forces and moments. The idea is to evaluate the forces that act on the rod, both internally and externally. This is done via *Newton's third law*, which states that if the rod is in equilibrium then the sum of external forces is equal to the sum of internal forces.

[6] Setting $\mathbf{d}_3(0) = (-1,0,0)$ and $\mathbf{d}_1(0) = (0,1,0)$ as one example, I arrive at $\mathbf{d}_3$ as in equation (2.9).

[7] Since I have assumed that the curve is unit-speed and the tangent vector of unit length, this automatically forces that the rod cannot be stretched.

2.3.1 Stabilising the Forces

By taking a segment of the rod, the forces acting on it can be investigated. Let the segment of the rod be defined by the range $[s, L]$ with an arbitrary s; then at s, three individual forces act on the rod. A force $\mathbf{n}(s)$ is exerted externally by the material of the rod on the segment $[0, s)$; another force $\mathbf{N}$, independent of s, acts on the end point of the rod. By Newton's laws, the sum of these two forces is equal to the sum of internal forces, which can be defined as a group of force densities $\mathbf{f}(s)$ acting on the interior of the range $[s, L)$. Quantitatively that is,

$$\mathbf{n}(s) + \mathbf{N} = \int_s^L \mathbf{f}(s')\ \mathrm{d}s', \tag{2.12}$$

and by differentiation is equivalent to,

$$\frac{d\mathbf{n}}{ds} = -\mathbf{f}(s). \tag{2.13}$$

Here, I have denoted $\mathbf{f}(s)$ as the generalised internal forces acting on the rod, having usually arisen physically from friction due to viscosity within a medium or even resistance from induction into an electromagnetic field. Below, Figure (2.2) demonstrates the forces and how they act on a generalised subsection of rod, this also includes moments and couples, which I now look to evaluate.

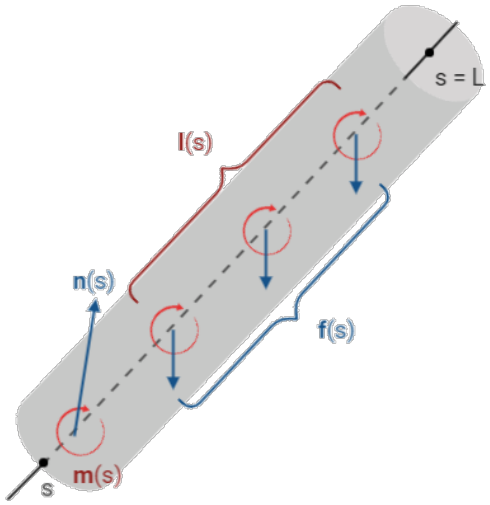

Figure 2.2: Figure showing the forces, moments and couples acting on a generalised subsection of rod.

2.3.2 Balancing Moments and Couples

Should one once again consider the $[s, L]$ segment of the rod, three explicit moments that act on a specific point in space can be evaluated. Denoting this general point $\mathbf{p}$ with arbitrary s as before, the moment experienced at s is $[\mathbf{r}(s) - \mathbf{p}] \times \mathbf{n}(s)$. Similarly at the end point of the rod ($\mathbf{r}(L)$) a moment $[\mathbf{r}(L) - \mathbf{p}] \times \mathbf{N}$ is applied. Since the internal force $\mathbf{f}(s)$ acts at every point along the rod, I define the moment generated by $\mathbf{f}$ as the density $[\mathbf{r}(s) - \mathbf{p}] \times \mathbf{f}(s)$ per unit length.

Couples do not produce a net force, but produce a moment, as the forces applied do not act at the same point. This is the reason that the rod may twist when forces are applied. A couple $\mathbf{m}(s)$ acting around the point s is generated by the material of the rod acting on the section $[0, s)$, with $\mathbf{M}$ the couple acting on $\mathbf{r}(L)$. The final couple density $\mathbf{l}(s)$ exerts on the subsection $[s, L)$. Then, by the third law of Newton,

$$[\mathbf{r}(s) - \mathbf{p}] \times \mathbf{n}(s) + [\mathbf{r}(L) - \mathbf{p}] \times \mathbf{N} + \mathbf{m}(s) + \mathbf{M} = \int_s^L [\mathbf{r}(s') - \mathbf{p}] \times \mathbf{f}(s) + \mathbf{l}(s') \, \mathrm{d}s'.$$

By taking the total derivative of this equation with respect to s,

$$[\mathbf{r}(s) - \mathbf{p}] \times \frac{d\mathbf{n}}{ds} + \frac{d\mathbf{r}}{ds} \times \mathbf{n} + \frac{d\mathbf{m}}{ds} = -[\mathbf{r}(s) - \mathbf{p}] \times \mathbf{f}(s) - \mathbf{l}(s); \tag{2.14}$$

as a result of force equilibrium (2.13),

$$\frac{d\mathbf{r}}{ds} \times \mathbf{n} + \frac{d\mathbf{m}}{ds} = -\mathbf{l}(s). \tag{2.15}$$

Together with the definition of the tangential vector $\mathbf{d}_3$, the following system can describe the balance of the rod in its entirety,

$$\begin{aligned} \frac{d\mathbf{n}}{ds} + \mathbf{f} &= \mathbf{0}, \\ \frac{d\mathbf{m}}{ds} + \mathbf{d}_3 \times \mathbf{n} + \mathbf{l} &= \mathbf{0}. \end{aligned} \tag{2.16}$$

Whilst these equations describe the rod in equilibrium, they cannot show how a rod may develop throughout time. Often mathematicians assume that the system can be modelled as quasi-static to introduce time dependence, but in general this is not the case. Quasi-static processes happen at such a rate that the internal equilibrium of the system remains constant. Yet, in many cases of rod theory, this should not be assumed, as the process happens relatively fast. This is where I rely on the dynamic Kirchhoff rod equations to further the model.

Section 3

Kirchhoff's Elastic Rod Theory

The equations (2.16) above are an example of a system that describes the behaviour of a Kirchhoff elastic rod in equilibrium. However, in order to find solutions that progress through time, a system that has explicit time dependence is necessary. Kirchhoff's elastic theory describes equations that demonstrate the dynamics of an inextensible rod with a central curve $\mathbf{r}$, written as an extension of the equilibrium case just derived.

For a Kirchhoff rod described by a moving frame basis[8], the following system arises due to conservation of linear momentum (3.1) and angular momentum (3.2) of the rod, where ρ is the material density and I_1, I_2 are the second moments of area[9] in the $\mathbf{d}_1, \mathbf{d}_2$ directions respectively.

$$\frac{\partial \mathbf{n}}{\partial s} + \mathbf{f} = \rho \frac{\partial^2 \mathbf{r}}{\partial t^2} \tag{3.1}$$

$$\frac{\partial \mathbf{m}}{\partial s} + \mathbf{d}_3 \times \mathbf{n} + \mathbf{l} = \rho \left(I_1 \mathbf{d}_1 \times \frac{\partial^2 \mathbf{d}_1}{\partial t^2} + I_2 \mathbf{d}_2 \times \frac{\partial^2 \mathbf{d}_2}{\partial t^2} \right) \quad [10] \tag{3.2}$$

3.1 Simplifying Assumptions

In its current state, the system cannot be solved. At present, there are a total of 15 functions that need to be satisfied. As a consequence, some safe assumptions must be made about the system to reduce the number of unknown quantities. By initially ignoring any internal forces $\mathbf{f}$ and couple densities $\mathbf{l}$, the number of quantities is reduced by 6 and one can further

[8] This system is defined with respect to the basis vectors $\mathbf{d}_1, \mathbf{d}_2, \mathbf{d}_3$.

[9] Second moments of area describe a rods resistance to applied forces in a particular direction, also known as the area moment of inertia.

assume that the generalised couple $\mathbf{m}(s)$ takes the form: $\mathbf{m} = Au_1\mathbf{d}_1 + Bu_2\mathbf{d}_2 + Cu_3\mathbf{d}_3$, where the constants A, B, C are given, but depend on the material structure[10]. More for simplicity, if the assumption that the quantities I_1 and I_2 are equal is made, this suggests that the rod bends equally in all directions, implying a circular cross-section. The system (3.1), (3.2) now reduces to,

$$\frac{\partial \mathbf{n}}{\partial s} = \rho \frac{\partial^2 \mathbf{r}}{\partial t^2}, \tag{3.3}$$
$$\frac{\partial \mathbf{m}}{\partial s} + \mathbf{d}_3 \times \mathbf{n} = \rho I \left(\mathbf{d}_1 \times \frac{\partial^2 \mathbf{d}_1}{\partial t^2} + \mathbf{d}_2 \times \frac{\partial^2 \mathbf{d}_2}{\partial t^2} \right),$$

where the aim is to directly solve for $\mathbf{r}(s)$. Taking the planar assumption[11] as previously described in Section 2.2,

$$\frac{\partial \mathbf{n}}{\partial s} = \frac{\partial}{\partial s}\left(n_1\mathbf{d}_1 + n_2\mathbf{d}_2 + n_3\mathbf{d}_3\right) = \left(\frac{\partial n_1}{\partial s}\mathbf{d}_1 + n_1\frac{\partial \mathbf{d}_1}{\partial s} + \frac{\partial n_2}{\partial s}\mathbf{d}_2 + n_2\frac{\partial \mathbf{d}_2}{\partial s} + \frac{\partial n_3}{\partial s}\mathbf{d}_3 + n_3\frac{\partial \mathbf{d}_3}{\partial s} \right).$$

Then, by the definition of the basis vectors in equation (2.9), the first-order partial derivatives are represented as follows,

$$\frac{\partial \mathbf{d}_1}{\partial s} = -\frac{\partial \theta}{\partial s}\mathbf{d}_3, \quad \frac{\partial \mathbf{d}_2}{\partial s} = \mathbf{0}, \quad \frac{\partial \mathbf{d}_3}{\partial s} = \frac{\partial \theta}{\partial s}\mathbf{d}_1. \tag{3.4}$$

This further implies the partial derivative of the force $\mathbf{n}$ is given by:

$$\frac{\partial \mathbf{n}}{\partial s} = \left(\frac{\partial n_1}{\partial s} + n_3\frac{\partial \theta}{\partial s} \right)\mathbf{d}_1 + \frac{\partial n_2}{\partial s}\mathbf{d}_2 + \left(\frac{\partial n_3}{\partial s} - n_1\frac{\partial \theta}{\partial s} \right)\mathbf{d}_3. \tag{3.5}$$

3.2 Solving the System

Henceforth, the objective will be to express $\frac{\partial^2 \mathbf{r}}{\partial t^2}$ in terms of the basis vectors. Should one differentiate the equation (2.11) twice with respect to a time t, it follows that,

$$\frac{\partial^2 \mathbf{r}}{\partial t^2} = \int_0^s \left(\frac{\partial^2 \theta}{\partial t^2}\mathbf{d}_1 - \left(\frac{\partial \theta}{\partial t} \right)^2 \mathbf{d}_3 \right) \mathrm{d}s'. \tag{3.6}$$

[10] Area moments of inertia are in fact proportional to the bending coefficients A, B, C, related by a material specific constant E known as the Young's modulus. I look into this in further detail in Section 4.

[11] Quantitatively, $u_1 = u_3 = 0$.

Observing the first equation of (3.3), as just described, equation of coefficients of the linear independent basis vectors is not trivial, since integration of the basis vectors is imperative when making a comparison to (3.6). The first equation of (3.3) can be expanded in the following way,

$$\left(\frac{\partial n_1}{\partial s}+n_3\frac{\partial\theta}{\partial s}\right)\mathbf{d}_1+\frac{\partial n_2}{\partial s}\mathbf{d}_2+\left(\frac{\partial n_3}{\partial s}-n_1\frac{\partial\theta}{\partial s}\right)\mathbf{d}_3=\rho\int_0^s\left(\frac{\partial^2\theta}{\partial t^2}\mathbf{d}_1-\left(\frac{\partial\theta}{\partial t}\right)^2\mathbf{d}_3\right)\mathrm{d}s'. \quad (3.7)$$

Reducing the complication of the integral can be achieved by the Leibniz rule; differentiating the above equality produces the equality below.

$$\begin{aligned}&\left(\frac{\partial^2 n_1}{\partial s^2}+\frac{\partial^2\theta}{\partial s^2}n_3+\frac{\partial n_3}{\partial s}\frac{\partial\theta}{\partial s}\right)\mathbf{d}_1+\left(\frac{\partial n_1}{\partial s}+n_3\frac{\partial\theta}{\partial s}\right)\frac{\partial\mathbf{d}_1}{\partial s}\\ +\ &\left(\frac{\partial^2 n_3}{\partial s^2}-\frac{\partial^2\theta}{\partial s^2}n_1-\frac{\partial n_1}{\partial s}\frac{\partial\theta}{\partial s}\right)\mathbf{d}_3+\left(\frac{\partial n_3}{\partial s}-n_1\frac{\partial\theta}{\partial s}\right)\frac{\partial\mathbf{d}_3}{\partial s} \quad (3.8)\\ =\ &\rho\frac{\partial^2\theta}{\partial t^2}\mathbf{d}_1-\rho\left(\frac{\partial\theta}{\partial t}\right)^2\mathbf{d}_3\end{aligned}$$

Now by comparing coefficients of the basis vectors, with their derivatives defined in (3.4), it follows that,

$$\frac{\partial^2 n_1}{\partial s^2}+\frac{\partial^2\theta}{\partial s^2}n_3+2\frac{\partial n_3}{\partial s}\frac{\partial\theta}{\partial s}-n_1\left(\frac{\partial\theta}{\partial s}\right)^2=\rho\frac{\partial^2\theta}{\partial t^2}, \quad (3.9)$$

$$\frac{\partial n_2}{\partial s}=0, \quad (3.10)$$

$$\frac{\partial^2 n_3}{\partial s^2}-\frac{\partial^2\theta}{\partial s^2}n_1-2\frac{\partial n_1}{\partial s}\frac{\partial\theta}{\partial s}-n_3\left(\frac{\partial\theta}{\partial s}\right)^2=-\rho\left(\frac{\partial\theta}{\partial t}\right)^2. \quad (3.11)$$

Now focusing on the second equation of the system (3.3), with the triad of orthonormal vectors, it is possible to notice that in this case,

$$\mathbf{d}_1\times\frac{\partial^2\mathbf{d}_1}{\partial t^2}+\mathbf{d}_2\times\frac{\partial^2\mathbf{d}_2}{\partial t^2}=\frac{\partial^2\theta}{\partial t^2}\mathbf{d}_2. \quad (3.12)$$

This reduces the second equation of (3.3) to:

$$\frac{\partial\mathbf{m}}{\partial s}+\mathbf{d}_3\times\mathbf{n}=\rho I\frac{\partial^2\theta}{\partial t^2}\mathbf{d}_2. \quad (3.13)$$

Comparing the $\mathbf{d}_2$ component of each term and assuming $\mathbf{m}$ takes the form as previously

stated, using (2.4) to observe $u_2 = \frac{\partial \theta}{\partial s}$ provides the equality:

$$B\frac{\partial^2 \theta}{\partial s^2} + n_1 = \rho I \frac{\partial^2 \theta}{\partial t^2}. \tag{3.14}$$

Under these assumptions, the system (3.3) then reduces to the form shown below.

$$\frac{\partial^2 n_1}{\partial s^2} + \frac{\partial^2 \theta}{\partial s^2} n_3 + 2\frac{\partial n_3}{\partial s}\frac{\partial \theta}{\partial s} - n_1 \left(\frac{\partial \theta}{\partial s}\right)^2 = \rho \frac{\partial^2 \theta}{\partial t^2} \tag{3.15}$$

$$B\frac{\partial^2 \theta}{\partial s^2} + n_1 = \rho I \frac{\partial^2 \theta}{\partial t^2} \tag{3.16}$$

$$\frac{\partial^2 n_3}{\partial s^2} - \frac{\partial^2 \theta}{\partial s^2} n_1 - 2\frac{\partial n_1}{\partial s}\frac{\partial \theta}{\partial s} - n_3 \left(\frac{\partial \theta}{\partial s}\right)^2 = -\rho \left(\frac{\partial \theta}{\partial t}\right)^2 \tag{3.17}$$

In order to solve this system, a specific type of solution can be expected, namely periodic and oscillatory behaviours of the parameter s. But if the assumption is made that the curvature of the rod $\kappa = \frac{\partial \theta}{\partial s}$ stays comparatively small, the non-linear terms consisting of $\left(\frac{\partial \theta}{\partial s}\right)^2$ vanish, reducing the complexity of the system considerably.

Conjecture.

> Any function defined on the real line can be represented by a Fourier series if it is periodic.

In this case, I can assume that the forms of the periodic functions are written as Fourier series as below.

$$\theta(s,t) = \sum_{m=1}^{\infty} a_{1m}(s)\cos(mPt) + a_{2m}(s)\sin(mPt), \tag{3.18}$$

$$n_1(s,t) = \sum_{m=1}^{\infty} b_{1m}(s)\cos(mPt) + b_{2m}(s)\sin(mPt),$$

$$n_3(s,t) = \sum_{m=1}^{\infty} c_{1m}(s)\cos(mPt) + c_{2m}(s)\sin(mPt).$$

Here the constants m and P determine the number of modes and periodicity respectively. As an example, evaluating (3.16) using the linear independence of the trigonometric functions,

$$B\frac{\mathrm{d}^2 a_{1m}}{\mathrm{d}s^2} + b_{1m}(s) = -\rho I P^2 m^2 a_{1m}, \tag{3.19}$$

$$B\frac{\mathrm{d}^2 a_{2m}}{\mathrm{d}s^2} + b_{2m}(s) = -\rho I P^2 m^2 a_{2m}. \tag{3.20}$$

For equation (3.17), the right side can be expanded as,

$$-m^2 P^2 \rho \left[a_{1m}^2 \sin^2(mPt) - 2a_{1m}a_{2m}\cos(mPt)\sin(mPt) + a_{2m}^2\cos^2(mPt)\right]. \tag{3.21}$$

This means coefficients of the $\cos(mPt)$ and $\sin(mPt)$ terms above can be compared, to find that the second partial derivative of n_3 vanishes, that is,

$$\frac{d^2 c_{1m}}{ds^2}\cos(mPt) + \frac{d^2 c_{2m}}{ds}\sin(mPt) = 0 \implies \frac{\partial^2 n_3}{\partial s^2} = 0, \tag{3.22}$$

Instead, comparing the $\cos^2(mPt)$, $\sin^2(mPt)$ and $\sin(2mPt)$ terms respectively, produces the three following identities,

$$\begin{aligned}
\frac{d^2 a_{1m}}{ds^2}b_{1m} + 2\frac{db_{1m}}{ds}\frac{da_{1m}}{ds} &= m^2 P^2 \rho a_{2m}^2, \\
\frac{d^2 a_{2m}}{ds^2}b_{2m} + 2\frac{db_{2m}}{ds}\frac{da_{2m}}{ds} &= m^2 P^2 \rho a_{1m}^2, \\
\frac{d^2 a_{1m}}{ds^2}b_{2m} + \frac{d^2 a_{2m}}{ds^2}b_{1m} + 2\frac{db_{2m}}{ds}\frac{da_{1m}}{ds} + 2\frac{db_{1m}}{ds}\frac{da_{2m}}{ds} &= -2m^2 P^2 \rho a_{1m}a_{2m}.
\end{aligned} \tag{3.23}$$

Similarly for the equation (3.15) it is now possible to notice,

$$\rho\frac{\partial^2\theta}{\partial t^2} = -\rho m^2 P^2\left[a_{1m}\cos(mPt) + a_{2m}\sin(mPt)\right]. \tag{3.24}$$

Once again by the linear independence of the periodic functions,

$$2\frac{\partial n_3}{\partial s}\frac{\partial\theta}{\partial s} + n_3\frac{\partial^2\theta}{\partial s^2} = 0 \tag{3.25}$$

$$\implies \quad \frac{\partial^2 n_1}{\partial s^2} = \rho\frac{\partial^2\theta}{\partial t^2}. \tag{3.26}$$

In terms of the Fourier series coefficients, that is,

$$\frac{d^2 b_{1m}}{ds^2} = -m^2 P^2 \rho a_{1m}, \tag{3.27}$$
$$\frac{d^2 b_{2m}}{ds^2} = -m^2 P^2 \rho a_{2m}.$$

Under the assumption that c_{1m} and c_{2m}, which are linear from (3.22), are actually zero, then,

$$a_{1m} = -\frac{1}{m^2 P^2 \rho}\frac{d^2 b_{1m}}{ds^2}, \quad a_{2m} = -\frac{1}{m^2 P^2 \rho}\frac{d^2 b_{2m}}{ds^2}. \tag{3.28}$$

Differentiating the equation (3.16) twice with respect to s produces,

$$B\frac{\partial^4 \theta}{\partial s^4} + \frac{\partial^2 n_1}{\partial s^2} = \rho I \frac{\partial^2}{\partial s^2}\left(\frac{\partial^2 \theta}{\partial t^2}\right) \tag{3.29}$$

$$\implies \quad B\frac{\partial^4 \theta}{\partial s^4} + \frac{\partial^2 n_1}{\partial s^2} = -m^2 P^2 \rho I \frac{\partial^2 \theta}{\partial s^2}\left(a_{1m}\cos(mPt) + a_{2m}\sin(mPt)\right) \tag{3.30}$$

$$\implies \quad B\frac{\partial^4 \theta}{\partial s^4} + \rho\frac{\partial^2 \theta}{\partial t^2} - \rho I \frac{\partial^4 \theta}{\partial s^2 \partial t^2} = 0 \tag{3.31}$$

By the equations (3.28), substituting into (3.19) and (3.20) eliminates a_{1m} and a_{2m} from the system, implying,

$$\frac{B}{m^2 P^2 \rho}\frac{d^4 b_{1m}}{ds^4} + I\frac{d^2 b_{1m}}{ds^2} - b_{1m} = 0. \tag{3.32}$$

This is a fourth-order ordinary differential equation (ODE) that describes the system under all of the assumptions made.

3.2.1 Analytical ODE Solutions

Using traditional methods, I now look to solve the system in terms of an explicit analytical solution.

Let $\lambda_{\pm}^2 = \frac{m^2 P^2 \rho}{2B}\left(-I \pm \sqrt{I^2 + \frac{4B}{m^2 P^2 \rho}}\right)$ and $\alpha_{\pm} = \sqrt{\lambda_{\pm}^2}$, then the solution to the differential equation takes the form:

$$b_{1m} = \gamma_1 e^{s\alpha_+} + \gamma_2 e^{s\alpha_-} + \gamma_3 e^{-s\alpha_+} + \gamma_4 e^{-s\alpha_-}, \;\; \gamma_i \in \mathbb{R} \;\forall\; i \in [1,4], \tag{3.33}$$

which is an equally valid solution for b_{2m} by symmetry, that is,

$$b_{2m} = \delta_1 e^{s\alpha_+} + \delta_2 e^{s\alpha_-} + \delta_3 e^{-s\alpha_+} + \delta_4 e^{-s\alpha_-}, \;\; \delta_i \in \mathbb{R} \;\forall\; i \in [1,4]. \tag{3.34}$$

It follows that,

$$a_{1m} = \frac{-1}{m^2P^2\rho}\left(\gamma_1\alpha_+^2 e^{s\alpha_+} + \gamma_2\alpha_-^2 e^{s\alpha_-} + \gamma_3\alpha_+^2 e^{-s\alpha_+} + \gamma_4\alpha_-^2 e^{-s\alpha_-}\right), \tag{3.35}$$

$$a_{2m} = \frac{-1}{m^2P^2\rho}\left(\delta_1\alpha_+^2 e^{s\alpha_+} + \delta_2\alpha_-^2 e^{s\alpha_-} + \delta_3\alpha_+^2 e^{-s\alpha_+} + \delta_4\alpha_-^2 e^{-s\alpha_-}\right). \tag{3.36}$$

However, these solutions for a_{1m}, a_{2m}, b_{1m} and b_{2m} must also satisfy (3.15) and (3.16) which is equivalent to (3.23).

$$\frac{d^2a_{1m}}{ds^2} = \frac{-1}{m^2P^2\rho}\left(\gamma_1\alpha_+^4 e^{s\alpha_+} + \gamma_2\alpha_-^4 e^{s\alpha_-} + \gamma_3\alpha_+^4 e^{-s\alpha_+} + \gamma_4\alpha_-^4 e^{-s\alpha_-}\right), \tag{3.37}$$

$$\frac{d^2a_{2m}}{ds^2} = \frac{-1}{m^2P^2\rho}\left(\delta_1\alpha_+^4 e^{s\alpha_+} + \delta_2\alpha_-^4 e^{s\alpha_-} + \delta_3\alpha_+^4 e^{-s\alpha_+} + \delta_4\alpha_-^4 e^{-s\alpha_-}\right). \tag{3.38}$$

With the solutions above, one can then notice,

$$\frac{d^2a_{1m}}{ds^2}b_{1m} = \frac{db_{1m}}{ds}\frac{da_{1m}}{ds}, \tag{3.39}$$

$$\frac{d^2a_{2m}}{ds^2}b_{2m} = \frac{db_{2m}}{ds}\frac{da_{2m}}{ds}. \tag{3.40}$$

By using these equalities, the system (3.23) can be rearranged into the following form:

$$a_{2m}^2 = \frac{2}{m^2P^2\rho}\frac{d^2a_{1m}}{ds^2}b_{1m} \tag{3.41}$$

$$a_{1m}^2 = \frac{2}{m^2P^2\rho}\frac{d^2a_{2m}}{ds^2}b_{2m} \tag{3.42}$$

Evaluating these using equations (3.33)-(3.38) and once again assuming the linear independence of trigonometric functions, equating all coefficients of resulting exponential terms gives that,

$$\gamma_i = \sqrt{\frac{-\delta_i^2}{2}} \;\; \forall \;\; i \in [1,4]. \tag{3.43}$$

Given the assumption that all coefficients γ_i and δ_i were non-imaginary, I conclude that the only possible values that satisfy the system in this case are $\gamma_i = \delta_i = 0 \;\; \forall \;\; i$. Furthermore, this implies that, $a_{1m} = a_{2m} = b_{1m} = b_{2m} = 0$.

As no external body forces are applied to the rod, only a single (trivial) solution exists, which is: $\theta(s,t) = 0 = n_1(s,t)$. Graphically, this solution is represented by a straight rod

along an axis that neither bends, nor twists.

In order to obtain non trivial solutions, the idea of body forces $\mathbf{f}$ and torque densities $\mathbf{l}$ can be reintroduced. When defining the system previously, these values were fixed to zero for simplicity. Moreover, the system (3.1), (3.2) becomes,

$$\frac{\partial \mathbf{n}}{\partial s} + \mathbf{f} = \rho \frac{\partial^2 \mathbf{r}}{\partial t^2}, \tag{3.44}$$

$$\frac{\partial \mathbf{m}}{\partial s} + \mathbf{d}_3 \times \mathbf{n} + \mathbf{l} = \rho I \left(\mathbf{d}_1 \times \frac{\partial^2 \mathbf{d}_1}{\partial t^2} + \mathbf{d}_2 \times \frac{\partial^2 \mathbf{d}_2}{\partial t^2} \right),$$

where $\mathbf{f} = (f_1 \mathbf{d_1} + f_2 \mathbf{d_2} + f_3 \mathbf{d_3})$ and $\mathbf{l} = (l_1 \mathbf{d_1} + l_2 \mathbf{d_2} + l_3 \mathbf{d_3})$, the system is modified with the introduction of new terms,

$$\frac{\partial^2 n_3}{\partial s^2} - 2\frac{\partial n_1}{\partial s}\frac{\partial \theta}{\partial s} - n_1 \frac{\partial^2 \theta}{\partial s^2} - n_3 \left(\frac{\partial \theta}{\partial s} \right)^2 + \frac{\partial f_3}{\partial s} - f_1 \frac{\partial \theta}{\partial s} = -\rho \left(\frac{\partial \theta}{\partial t} \right)^2, \tag{3.45}$$

$$\frac{\partial^2 n_1}{\partial s^2} + 2\frac{\partial n_3}{\partial s}\frac{\partial \theta}{\partial s} + n_3 \frac{\partial^2 \theta}{\partial s^2} - n_1 \left(\frac{\partial \theta}{\partial s} \right)^2 + \frac{\partial f_1}{\partial s} + f_3 \frac{\partial \theta}{\partial s} = \rho \frac{\partial^2 \theta}{\partial t^2},$$

$$B \frac{\partial^2 \theta}{\partial s^2} + n_1 + l_2 = \rho I \frac{\partial^2 \theta}{\partial t^2}.$$

Regardless, while attempting to mathematically model such a system, I will assume that there exists some generalised internal force $\mathbf{f}$ and couple density $\mathbf{l}$ that satisfy the system as a whole. Should it also be assumed that the curvature doesn't grow too large (as assumed in the unforced case), the terms consisting of $\left(\frac{\partial \theta}{\partial s}\right)^2$ will dissipate.

I now look to adjust the system for the inclusion of a varied bending stiffness and observe alterations in behaviour.

Section 4

Variable Flexural Rigidity

"*The integrals which we have obtained are not only general expressions which satisfy the differential equation, they represent in the most distinct manner the natural effect which is the object of the phenomenon . . . when this condition is fulfilled, the integral is, properly speaking, the equation of the phenomenon; it expresses clearly the character and progress of it, in the same manner as the finite equation of a line or curved surface makes known all the properties of those forms.*"[11]

— Fourier, J. (1822)

This eloquent passage from Fourier accentuates the importance of integrals in the world around us. Spoken even before the conception of the elastica theory, this quote encapsulates the essence of the theory in its entirety.

In this section, I look at incorporating a variable bending stiffness according to thickness and solve the differential system via numerical integration as discussed by Xavier (2014) [12].

4.1 Explicit Derivation

With the system defined, I can begin to investigate the effects of changes in the bending stiffness within the rod. This is possible by varying B along the arc-length of the rod; stating

that it has explicit s dependence. I modify the dynamical derivation in the following way.[12]

$$B\frac{\partial^2\theta}{\partial s^2}+\frac{\partial\theta}{\partial s}\frac{\partial B}{\partial s}+n_1=\rho I\frac{\partial^2\theta}{\partial t^2} \tag{4.1}$$

Assuming $B\in C^1$, I return to solve the system. In terms of Fourier coefficients,

$$B(s)\frac{\mathrm{d}^2a_{1m}}{\mathrm{d}s^2}+B'(s)\frac{\mathrm{d}a_{1m}}{\mathrm{d}s}+b_{1m}(s)=-\rho IP^2m^2a_{1m}, \tag{4.2}$$

$$B(s)\frac{\mathrm{d}^2a_{2m}}{\mathrm{d}s^2}+B'(s)\frac{\mathrm{d}a_{2m}}{\mathrm{d}s}+b_{2m}(s)=-\rho IP^2m^2a_{2m}. \tag{4.3}$$

Since a_{1m} and a_{2m} are symmetric, I shall only solve for one and give the other a solution of the same form. Similar to before, a solvable fourth-order differential equation can be obtained:

$$\frac{B(s)}{m^2P^2\rho}\frac{d^4b_{1m}}{ds^4}+\frac{B'(s)}{m^2P^2\rho}\frac{\mathrm{d}^3b_{1m}}{\mathrm{d}s^3}+I\frac{d^2b_{1m}}{ds^2}-b_{1m}=0 \tag{4.4}$$

4.2 Physical Meaning

Since the physical meaning of a bending stiffness function is relatively arbitrary, I use the fact that the bending stiffness of the rod is in fact proportional to the area moment of inertia I[13]: that is $B=E\cdot I$, with proportionality constant E known as the flexural modulus. I shall assume the system is an ideal state, implying the flexural modulus is equivalent to the tensile modulus or Young's modulus.

$$E\frac{I(s)}{m^2P^2\rho}\frac{d^4b_{1m}}{ds^4}+E\frac{I'(s)}{m^2P^2\rho}\frac{\mathrm{d}^3b_{1m}}{\mathrm{d}s^3}+I(s)\frac{d^2b_{1m}}{ds^2}-b_{1m}=0, \tag{4.5}$$

Area moments of inertia can be explicitly calculated using the formula $I_x=\iint_R y^2\mathrm{d}y\mathrm{d}x$, by change of variables into polar coordinates, that is for a given radius R:

$$I_1=I_2=I=\int_0^R\int_{-\pi}^{\pi}R^3\sin\varphi\,\mathrm{d}\varphi\mathrm{d}R=\frac{\pi R^4}{4}. \tag{4.6}$$

Substituting this into the defining differential equation, I have an equation based on a radial

[12] I merge the l_2, $\frac{\partial f_1}{\partial s}$, $\frac{\partial f_2}{\partial s}$, $f_3\frac{\partial\theta}{\partial s}$ and $f_1\frac{\partial\theta}{\partial s}$ terms into the system and assume that some values of these will satisfy the system. Varying B will not affect the solution of the first two equations in (3.45).

[13] As in Section 3, I assumed that the cross-section was circular, so the principal bending stiffnesses are equal.

function $R(s)$ that can control the thickness of any given point s along the rod's profile.

$$\frac{\pi E}{4}\frac{R^4(s)}{m^2P^2\rho}\frac{d^4b_{1m}}{ds^4}+\frac{\pi E}{4}\frac{(R^4(s))'}{m^2P^2\rho}\frac{\mathrm{d}^3b_{1m}}{\mathrm{d}s^3}+\frac{\pi R^4(s)}{4}\frac{d^2b_{1m}}{ds^2}-b_{1m}=0 \tag{4.7}$$

4.3 Resolving a Solution

As shown in the unforced case, analytical solutions may exist. However, with more complex coefficients this is not always the case. Therefore, relying on approximate numerical solutions to the equation is crucial. Fortunately, in this case, the differential equations appear non-stiff, meaning any method is numerically stable and any deviation from the true solution is considered negligible (Goriely, Nizette and Tabor, 2001) [13].

By formulating the model in Python 3.9.2, I have implemented `scipy.integrate.odeint`[14] from the *scipy* package [14]. This makes use of a specific type of method, known as the implicit Adams-Bashforth method.

4.3.1 Adams Multistep Methods

These multistep methods use initial-valued boundary conditions to numerically generate interpolating polynomials. Given the differential equation,

$$y'(s)=f(s,y(s)), \tag{4.8}$$

the Adams-Bashforth method is specified by the iteration with error of order $\mathcal{O}(h^4)$, for ℓ_i the Lagrange polynomials [15]:

$$y_{n+m}=y_{n+m-1}+h\sum_{i=0}^{m-1}b_i f(s_{n+i},y_{n+i}),$$
$$b_i=\frac{1}{h}\int_0^h \ell_i(s_{n+m-1}+u)\,du.$$

With numerical solutions for b_{1m} and b_{2m}, using (2.11) and the following equivalence, resolving for $\mathbf{r}$ produces,

$$\theta(s,t)=-\frac{1}{m^2P^2\rho}\sum_{m=1}^{\infty}\left[\frac{d^2b_{1m}}{ds^2}(s)\cos(mPt)+\frac{d^2b_{2m}}{ds^2}\sin(mPt)\right]. \tag{4.9}$$

[14] Should the boundary conditions on the system change, it may be beneficial to change from an initial-value problem to a boundary-valued problem, such as `scipy.integrate.solve_bvp`, described in detail in Section 4.5.

To determine $\mathbf{r}$ from θ one must integrate. This requires that I use a method of numerical integration, given a specific number of steps.

4.3.2 Simpson's Rule for Numerical Integration

I use Simpson's rule for integration and evaluate at every s across the length of the rod, providing a set of Cartesian coordinates. This was possible, once again, by implementing the *scipy* package into the Python integrated development and learning environment (IDLE). This method makes use of the composite Simpson's rule, which evaluates subintervals as an alternative, to improve accuracy.

For a generic integral,

$$\int_a^b f(x)dx, \tag{4.10}$$

this can be approximated by the composite Simpson's method, with the interval $[a, b]$ dissected into n sub-intervals. For n even, $h = \frac{b-a}{n}$ and $x_j = a + jh$, $\exists\ \xi \in (a, b)$:

$$\int_a^b f(x)dx \approx \frac{h}{3}\left[f(a) + 2\sum_{j=1}^{n/2-1} f(x_{2j}) + \sum_{j=1}^{n/2} f(x_{2j-1}) + f(b)\right] - \frac{h^4}{180}(b-a)f^{(4)}(\xi) \tag{4.11}$$

The last error term in the formula is of order $\mathcal{O}(h^4)$. Using a suitable value of n steps, it is now possible to recreate the central curve $\mathbf{r}$.

Running the model requires a set of input variables that describe and determine the behaviour of the system, notably:

- the length: L ;
- modes and periodicity: m, P ;
- initial conditions: $\gamma = [\gamma_1, \gamma_2, \gamma_3, \gamma_4],\ \delta = [\delta_1, \delta_2, \delta_3, \delta_4]$;
- material density: ρ ;
- radial function: $R(s)$.

The initial conditions γ, δ, in particular, affect the solutions variously. In a physical sense, these conditions represent the starting state of the rod in the following way,

$$b_{1m}(0), \frac{db_{1m}}{ds}(0), \frac{d^2b_{1m}}{ds^2}(0), \frac{d^3b_{1m}}{ds^3}(0) = \gamma_1, \gamma_2, \gamma_3, \gamma_4, \tag{4.12}$$

$$b_{2m}(0), \frac{db_{2m}}{ds}(0), \frac{d^2b_{2m}}{ds^2}(0), \frac{d^3b_{2m}}{ds^3}(0) = \delta_1, \delta_2, \delta_3, \delta_4, \tag{4.13}$$

though at first glance do not represent translatable quantities.

$R(s)$ and L can be physically interpreted with ease; however, whilst I can vary the other parameters to observe changes in the solution, these are less visually interpretable, like the initial conditions. It is therefore important to clarify the impact that each parameter has on the solution and justify the validity of every decision when looking at real-world/physical examples.

4.4 Length Dependence

Before I begin to explicitly observe behaviours based on the radial function, I shall examine the effects that the other perceptible quantity, length, has. As in Figure (4.1) - that shows a simple exponentially decaying radius - this shows two nearly identical rods, with only the length being varied by a factor of 0.75. Despite only a minor difference in length, their behaviours differ quite significantly. The longer rod bends at a much greater rate than its counterpart, but the periodicities remain very similar, so it is apparent that the angular velocity at the end of each rod also varies significantly between the two simulations.

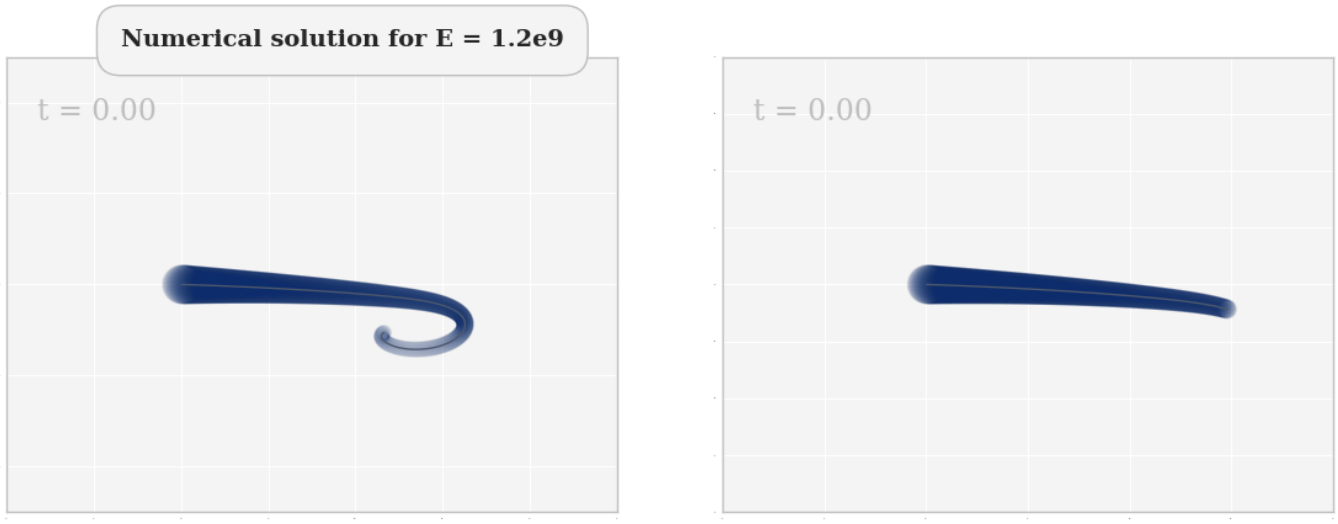

(a) **(b)**

Figure 4.1: Numerical time solutions of two rods with decaying exponential thicknesses. Both have identical parameters, with the exception of length. **(a)** $L = 2, m = 5, P = 1, \rho = 1.5, R(s) = 10e^{-s}, \boldsymbol{\gamma} = \boldsymbol{\delta} = [1, 1, 1, 1]$. https://kapwi.ng/c/yyOQR5aL. **(b)** $L = 1.5$. https://kapwi.ng/c/g52VAMEx.

For any general rod with a fixed initial position, this type of behaviour is to be expected and shall assume true; nevertheless, notwithstanding these observations, it may prove to be that a variation in the radial function plays a significant part in the dependence of length.

4.5 Boundary-Value Problems

The aforementioned initial conditions that initialise the system provide little physical understanding into how the rod should behave under these given conditions. This is because any initial condition for a fourth-order derivative in a complex system, such as this, is visually arbitrary. Upon looking at real-world examples, transforming to a boundary-valued problem enables the freedom to explicitly state directives for the rod, providing more intuitive and justifiable reasoning.

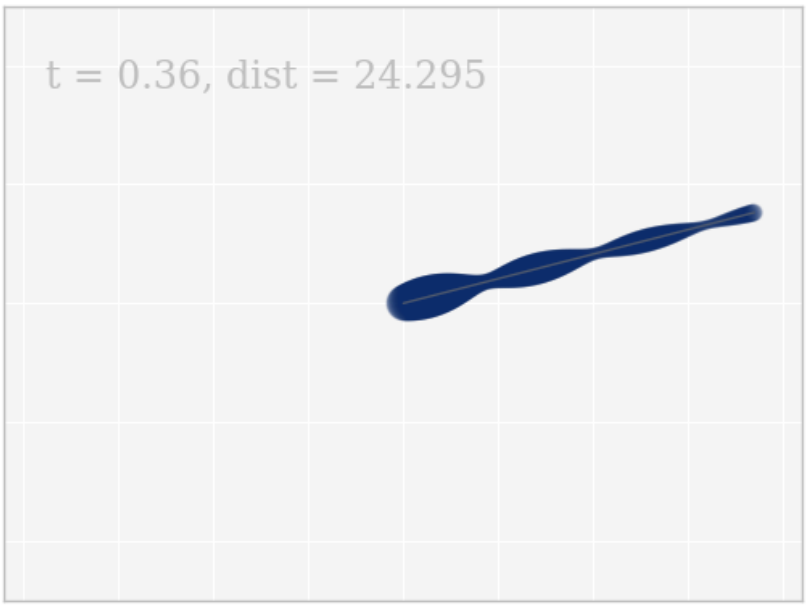

Figure 4.2: Numerical time solution of a rod with a varying sinusoidal thickness. $L = 2, m = 5, P = 3, \rho = 1.5, R(s) = 20e^{-s}\left(\sin(s) + 1.4\right)$. https://kapwi.ng/c/wi89YEjz

Figure (4.2) displays just how influential initial conditions can be to the model. Whilst the general bending motion in this case is monotonous, the boundary valued conditions provide a varying type of overarching behaviour. This example uses the following boundary

conditions to function:

$$\mathbf{r}(0) = 0, \quad \frac{d^2\mathbf{r}}{ds^2}(0) = 5, \quad \frac{d\mathbf{r}}{ds}(L) = 2, \quad \frac{d^2\mathbf{r}}{ds^2}(L) = 5.$$

The `integrate.solve_bvp` function from the *scipy* package used here implements a fourth-order collocation scheme, using a damped Newton method [16]. This allows the inclusion of boundary conditions at both ends of the rod. On the contrary, the initial value method gives the user greater control over the defining behaviour of the rod, particularly useful in classifying such actions.

Section 5

Categorical Solutions

In this section, I look to present the results of observations and numerical experiments, with a desire to categorise observed behaviours. I initially set out on improving a general model for the elastica theory in real-world applications, so shall thereafter, focus on physical applications of this mathematical model.

Although very specific parameters must be stated to initialise the simulation, this problem should only be of concern when looking to accurately represent real-world examples[(15)].

5.1 Types of Solutions

By varying the radial function R, it can be noticed that the rod exhibits substantially different behaviours based on the solution. In fact I notice two distinctive types of behaviours, a stabbing or prodding motion and a whipping type of motion.

5.1.1 Waving Motion

As a result of the assumption that solutions take a periodic form, all rods oscillate around a central line. This type of waving and stabbing motion usually only impacts the overall profile of the rod minimally. One particularly interesting case is a sinusoidal

[(15)] Typical values of the Young's modulus are given in these examples, solely to demonstrate the type of behaviour.

radial function as shown below in Figure (5.1)[16]. As the rod oscillates throughout time

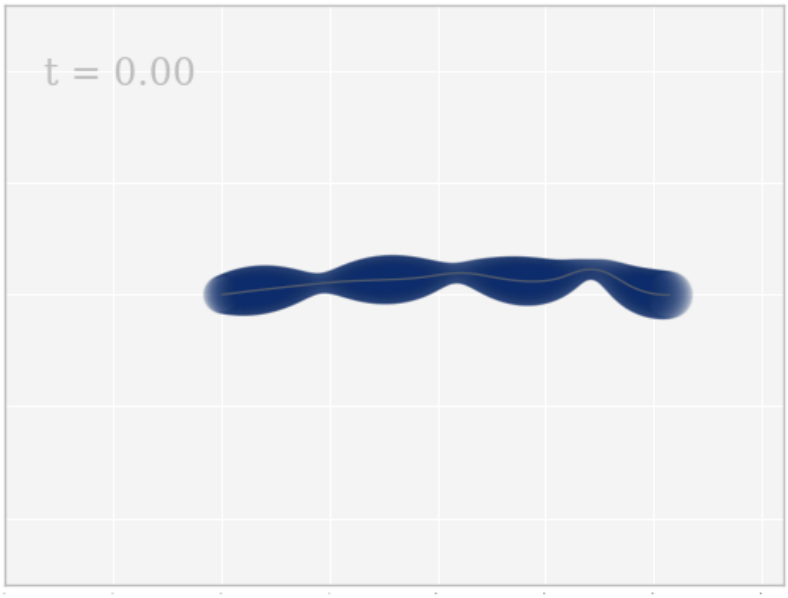

Figure 5.1: Numerical time solution of a rod with a varying sinusoidal thickness. $L = 2, m = 4, P = 1, \rho = 2, R(s) = 20\left(\sin(s) + 1.4\right), \boldsymbol{\gamma} = [3, 2, -2, 1], \boldsymbol{\delta} = [3, 2, 3, -10]$. https://kapwi.ng/c/PVfab1vz

it should become clear that it's structure does not curl or coil. Instead, as a result of the sections with smaller radii, the magnitude of displacement increases. Physically this is what is to be expected; these parts of the structure are typically weaker in comparison to sections with a larger radius, which deform at a reduced rate.

Should the forces applied be of ample magnitude, the rod may begin to buckle. Derived by Euler, the critical buckling load is proportional to the area moment of inertia, suggesting that as the radius decreases, the critical load limit lessens and it is more probable that buckling will occur [17]. It is also interesting to notice that the segments furthest from the fixed point deform substantially more, as a result of applied moments.

This type of motion occurs for a few different functions such as the hyperbolic cosine and stiff constant functions.

[16] The centre-line on which the entire behaviour of the rod is governed by is also shown in a lighter colour.

5.1.2 Whipping Motion

Whipping motion results in the formation of tight coils during oscillations. Similar to how a whip might behave, this type of motion often happens quicker than any other. As discussed previously, the smaller cross-sections begin to bend in a more extreme manner; so as the radial function of the rod decreases towards the end point, the segment furthest from the fixed point begins to coil and tighten - producing a type of whipping motion. Therefore, any monotonically decreasing function should, to some degree, exhibit this category of behaviour.

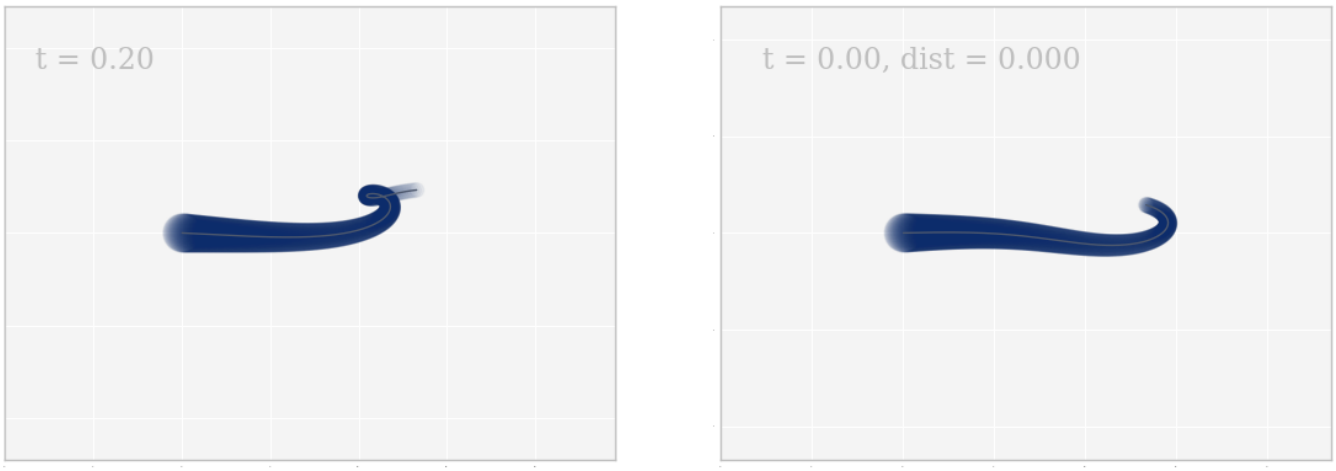

(a) **(b)**

Figure 5.2: Numerical time solutions of two rods, both with a decaying exponential thickness. **(a)** $L = 1.95, m = 5, P = 1, \rho = 2, R(s) = 10e^{-s}, \boldsymbol{\gamma} = [1, 1, 1, 1], \boldsymbol{\delta} = [1, 1, 0.8, -0.1]$. https://kapwi.ng/c/L08I0gbP.**(b)** $L = 1.93, m = 4.7, P = 2.3, \rho = 2, R(s) = 10e^{-s}, \boldsymbol{\gamma} = [0.2, 0.1, -0.1, 0], \boldsymbol{\delta} = [0.1, 2, 0.2, -0.5]$. https://kapwi.ng/c/ExmaD7pN

As shown in Figure (5.2a), the rod demonstrates a striking whip-like resemblance. However, since the assumption that the rod lies in a single three-dimensional plane was made, the overlap in fact causes this solution to be nullified. Even without the planar assumption, solutions like this can be extremely difficult to calculate, whilst introducing the concept of contact mechanics to model interactions the rod makes with itself.

On the contrary, this does not mean general solutions like this do not exist. By manipulating the input variables, any solution without a self-intersection can be justifiably valid as in Figure (5.2b). In this figure, I have also included the approximate magnitude of distance traced by the end point over one oscillation; this is to emphasise just how varied different behaviours can be.

5.2 Deviation from Constant Bending Stiffness

Refocusing on the motivation behind this project, authors of papers focusing on this style of elastica theory broadly assume a constant bending stiffness. Having studied two main types of motion, it is clear that a variable bending stiffness produces very different solutions. I, therefore, now aim to quantitatively verify this statement by comparing the two rods[17].

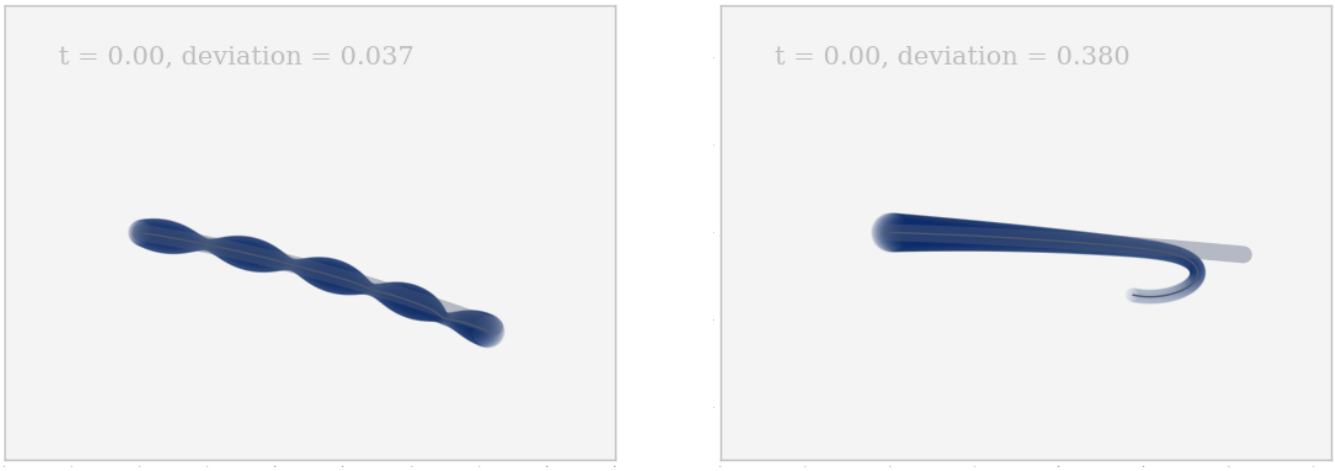

(a) **(b)**

Figure 5.3: Comparison solutions for constant radius function. **(a)** $L = 3, m = 5, P = 1, \rho = 4, R(s) = 3(\sin 9s + 1.3), \boldsymbol{\gamma} = [1, 2, 2, 1], \boldsymbol{\delta} = [1, 2, 2, 1]$. https://kapwi.ng/c/K7aSAokS. **(b)** $L = 2.1, m = 5, P = 1, \rho = 1.5, R(s) = 10e^{-s}, \boldsymbol{\gamma} = [0, 1, 1, 1], \boldsymbol{\delta} = [0, 1, 1, 1]$. https://kapwi.ng/c/CCXxhsXs

By initial observations of Figure (5.3a)[18], the general movement of the rod varies only slightly against the same rod with constant bending stiffness assumed[19]. In the case of a sinusoidally varying radius with roughly uniform behaviour, it can be justified to assume a constant radius. On the other hand, in Figure (5.3b) one can notice the maximum deviation of all corresponding points on each rod rises above 40% of its total length. This is a significant difference that can hardly be justified in any exponential decay example.

[17] The deviation between the two is measured as a proportion of length L and will be for all following animations.

[18] Providing the sinusoidal example with the same parameters as the exponential example, the deviation becomes negligible, so in this case is fairly uninteresting. I intentionally gave different parameters to highlight the fact that the sinusoidal case does in fact deviate from the constant case.

[19] As shown by the transparent rod superimposed behind.

5.3 Irregular Material Density

The flexural rigidity or bending stiffness of any object does not only depend on its thickness or radius; it can also rely on the internal structure of the rod. In all of the cases above, the assumption that the material density is constant was made; however, suppose that the internal structure is non-uniform, then this type of rod with a constant radial function may behave in a similar manner to the simulations already presented in this paper[20].

Having stated the dynamical Kirchhoff system, it is not possible to explicitly derive the full governing equation for a variable material density. However, similar to the assumptions made previously about curvature, I make the assumption that any new terms that should arise vanish. Directly, this means that any order of partial derivatives of ρ can be suitably ignored, assuming that the rate of change in ρ is insignificant. It is important to verify these conditions. The derivative of the function for ρ stated in the caption of Figure (5.4) is satisfactory, such that any derivative remains relatively small compared to other terms in the governing differential equation.

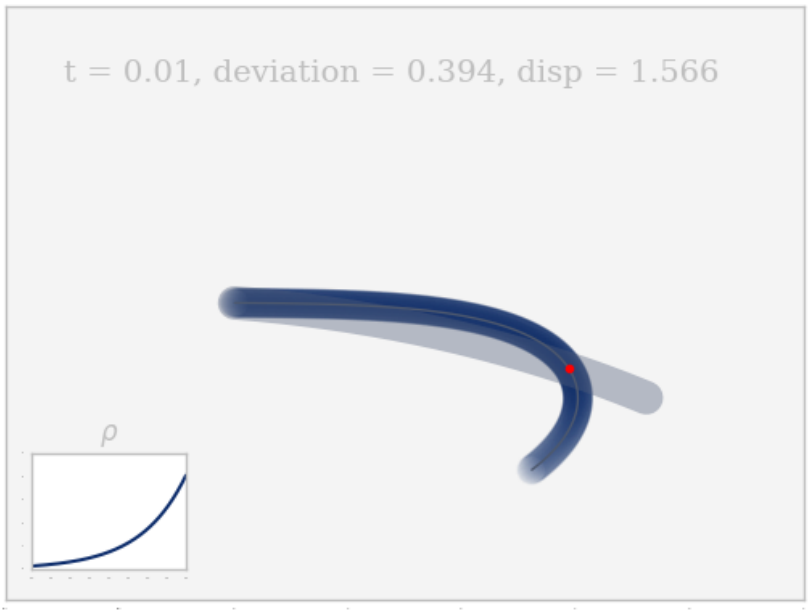

Figure 5.4: Numerical time solution of a rod with constant thickness but varied material density compared to a rod with both variables constant. $L = 2, m = 5, P = 1.3, \rho(s) = 0.8e^{1.2s-2}, R(s) = 10, \boldsymbol{\gamma} = [3, 1, 1, 2], \boldsymbol{\delta} = [1, 1, 1, 1]$. https://kapwi.ng/c/bzQffagr

[20] No adjustments to the system need to be made in order to accommodate this change. Simply stating a varied material density over the rods length will suffice under the following assumptions.

The example shown in Figure (5.4) demonstrates the dynamics of such a rod with varied material density. The density increases at an exponential rate, causing the end of the rod to oscillate with greater amplitude, whilst retaining the same periodicity. It is compared to a similar rod[19], with constant density $\rho = 2$. The point at which the densities are equivalent is represented by the red dot, where one can notice the dot steadily remaining on the central curve of the superimposed rod behind. Both observed rods have the same initial conditions, so the maximum, measured, absolute deviation between them is calculated along with the displacement of the varied rod from a central horizontal line, which both underline a fundamental change in behaviour.

In comparison to an exponential radial function example, similar to Figure (5.3b), the deviation from the constant case is relatively similar in Figure (5.4). However, providing this new rod with equivalent given conditions to Figure (5.3b), whilst varying the radius with the same density exponential function stated in Figure (5.4) and reverting to a uniform density, the change in geometry and curvature grows sufficient to violate the assumptions made when formulating the model. This implies they cannot be directly compared, yet it is clear to see that this variation in material density does not provide the same type of whipping motion as already categorised.

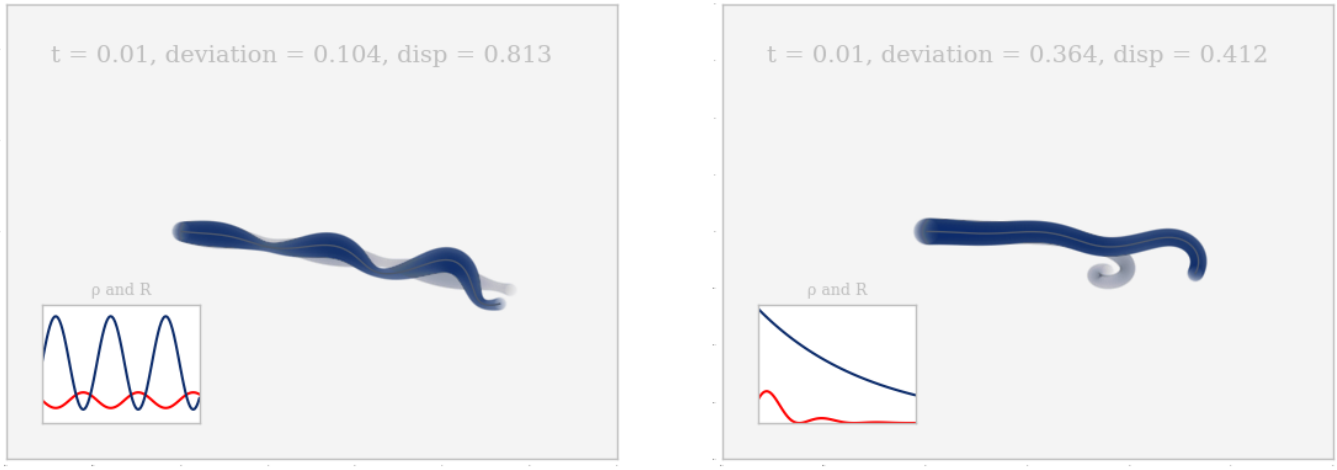

(a) **(b)**

Figure 5.5: **(a)** Numerical time solution of a rod with both varying sinusoidal thickness and material density. $L = 2, m = 5, P = 1.3, \rho(s) = 0.11(\sin(9s + \pi) + 3), R(s) = 3(\sin 9s + 1.3), \boldsymbol{\gamma} = \boldsymbol{\delta} = [1, 2, 2, 1], E = 1.2 \times 10^8$. https://kapwi.ng/c/tVwcBW0u. **(b)** Numerical time solution of a rod with varying exponential thickness and modified sinusoidal material density. $L = 1.5, m = 5, P = 1, \rho(s) = 0.7(\sin(9s + \pi) + 1)e^{-2.7s} + 0.1, R(s) = e^{2-0.7s}, \boldsymbol{\gamma} = [2, -0.4, 0, 2], \boldsymbol{\delta} = [3, 0.2, 1, -4], E = 1.2 \times 10^8$. https://kapwi.ng/c/KDK2ZqW2. (ρ in red, R in blue).

Often structures are made of composite materials and are not always uniformly dense. The combination of both a varied material density and variable thickness poses a new, interesting behaviour. Figure (5.5) illustrates the numerical time solutions of rods both with sinusoidally-varying material densities, while Figure (5.5a) shows a sinusoidal thickness and Figure (5.5b) demonstrates an exponential radial function.

Figure (5.5a) is constructed in such a way that the structure of material density accentuates the typical sinusoidal behaviour. The sections of thinner radius oscillate at an increased rate, where the superimposed sinusoid with constant material density acts almost as an averaged curve through the rod. The deviation (again measured as a proportion of length) between the two attains its maximum at the limit of its oscillation.

The more interesting behaviour arises from the combination of exponential thickness and sinusoidally decaying material density. Shown by Figure (5.5b), the rod begins to exhibit both features from the waving and whipping motion. In comparison to the constant material density case (superimposed behind), the end point of the rod coils significantly less, as a direct result of the varied density. On the other hand, the magnitude of deviation is notably larger in this case and in fact does not occur at the limit of oscillation.

Section 6

Relating to Real-World Examples

Given several specific types of solutions, there are similar patterns of how objects in the real-world behave. However, for these solutions to be physically accurate, it must be remembered that certain forces $\mathbf{f}$ and $\mathbf{l}$ must act on the system to satisfy it. This means that any example must have realistic forces acting on it. Such forces may include fluid viscosity or a magnetic inductive force.

Most physical examples represented by this model occur within viscous fluids, such as water or blood. The force generated by viscosity is proportional to the velocity gradient and area, so provides suitable values for the generalised internal forces $\mathbf{f}$ and couple densities $\mathbf{l}$.

However, one variable used to initialise the system is the flexural modulus, which, as assumed previously, is equivalent to the Young's modulus. This is a material property based on its ability to withstand tension or compression. Values for most materials lie in a range between 0.01 GPa and 1000 GPa, with common values cited by Helmenstine (2021) [18], so it is therefore important to state a value in every case. This quantity must be physically determined in every situation, which in this project is not always possible; therefore, I use known values similar to the example chosen to represent the material in question. The models in the previous section have also been provided with a suitable Young's modulus value to emphasise the defining motion in each case.

These values for the flexural modulus can be applied to several real-world examples. Below, I endeavour to explore the types of categorical behaviours in the instance of biological applications, as well as the consideration between form and function.

6.1 Crustacean Antennae

Antennae in crustaceans is an example of serial homology (University of California Museum of Paleontology [19]). All crustaceans have two appendages in common, namely antennules and secondary antennae, with the latter having greater length. The precise purposes of these appendages are not fully known; they are primarily used for sensory, but are also thought to be used in communication and enhancing stability (Boxshall, 2013) [20] and (Vickery, Hollowell and Hughes, 2012) [21].

The general structure of crustacean antennae is composed of many sections known as flagellum, distinctly controlling the behaviour of its movement. Although antennae naturally occur in various shapes, they can be generally described by a decaying sinusoidal function as shown in Figure (6.1a).

The approximation in Figure (6.1b) is a perfect example of the waving motion described in the previous section. It is clear to observe that the magnitude of oscillations remain relatively small; yet, as expected, the structure tends to bend at a greater rate where the radius is minimised, combining behaviours of both types of motion described previously.

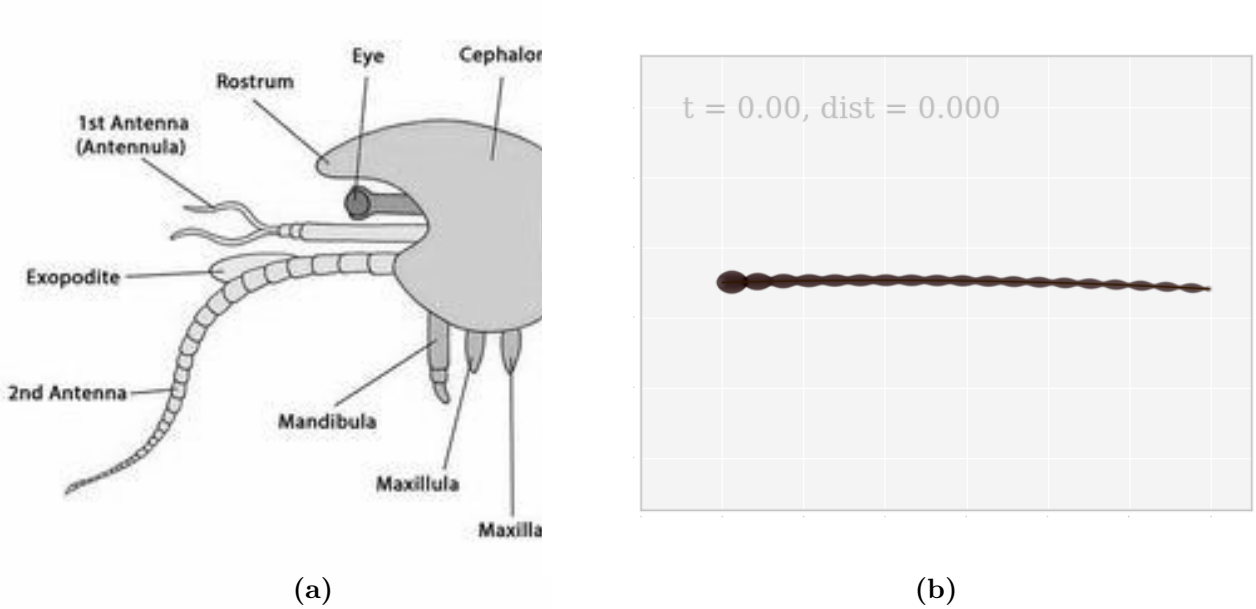

(a) **(b)**

Figure 6.1: **(a)** Biological structure of crustaceans. [22] **(b)** Numerical time solution of a rod with decaying exponential thickness, representing crustacean secondary antennae. $L = 6, m = 4, P = 1, \rho = 0.5, R(s) = \left(e^{2-3s} + 1\right)\left(\sin\left(20s - 1\right) + 1\right) - 0.3s + 2, \boldsymbol{\gamma} = [3, 2, -2, 1], \boldsymbol{\delta} = [3, 2, 3, -10], E = 0.8 \times 10^9$. https://kapwi.ng/c/8fCrxssv.

Although an approximate radial function can easily be suggested, a value for the Young's modulus of the material must be defined. Based on similar known values, I provide the

model with a value based on the stress/strain ratio of low-density polyethylene (LDPE) (0.8×10^9 Pa) for the antenna, where the structure of antennae is discussed in more detail by Loudon (2005) in the paper titled: 'Flexural Stiffness of Insect Antennae' [23].

Concerning functionality, the antenna may need to become flexible, particularly if used in stability. This may also need to become rigid in the onset of strong underwater currents. Incorporating both factors, perhaps leads to the reasoning behind the geometric structure displayed above.

6.2 Sperm Cells

Sperm cells and crustacean antennae are very contrasting examples, but can both be modelled using exponential functions. This time I model the cell using a Gaussian function, rather than including any periodic function as before.

However, unlike the antennae, the reason sperm cells are shaped in the way that they are, is for efficiency in movement. The body is streamlined, where the head narrows in an attempt to reduce drag upon movement through a fluid (MicroscopeMaster.com) [24]. As already seen, exponential functions produce whipping motion, which in the case of movement,

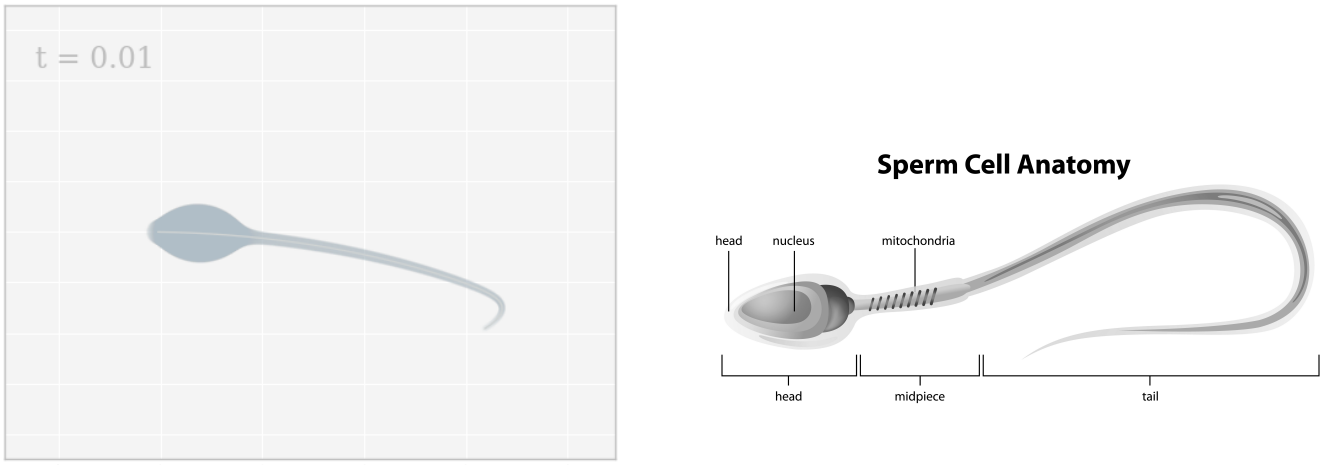

(a) **(b)**

Figure 6.2: **(a)** Numerical time solution of a rod with a modified Gaussian function thickness, representing the behaviour of a sperm cell. $L = 4, m = 6, P = 4, \rho = 0.3, R(s) = 27e^{-(-3.7s+1.5)^2} - 0.3s + 1.4, \boldsymbol{\gamma} = [3, 0.5, 0.5, 3], \boldsymbol{\delta} = [-2, -5, 1, 5], E = 0.07 \times 10^9$. https://kapwi.ng/c/cZkKxhJA. **(b)** Biological structure of a sperm cell. [25]

generates velocity in an efficient manner by displacing the fluid particles to propel itself.

This is shown by the sheer magnitude of oscillations exhibited by the tail of the sperm cell; this exaggerated whipping motion is typical of sperm cells, where the model had been provided (as a variable in Equation (4.7)) with a smaller value for the Young's modulus (0.07×10^9 Pa) to introduce this motion.

Notice in Figure (6.2a) the head remains relatively still in comparison to the tail, this is important as sperm cells need to travel in a particular direction. Ensuring the head is stable keeps the cell on course. As seen previously, wider sections tend to resist bending at a greater rate. While the head contains the nucleus and other important parts, this observation may also justify why sperm are shaped in this unique way.

6.3 Octopus Tentacles

Similar to antennae, tentacles are attached to a (relatively) fixed body, unlike sperm cells, which, as a single entity, move through fluids and are free to bend in any direction[(21)].

The arms, to be biologically meticulous, have various functions for the invertebrate. Despite the similarity in appearance, the back two arms are used, primarily, for movement; whilst the other six can also enable movement, they are used for grabbing prey and are sensory (Hall n.d.) [26].

Unlike the previous examples, octopus tentacles have a more complex internal structure, which for the purpose here is to be assumed uniform. However, it may more accurately be modelled using a varied material density as discussed in Section (5.3). As a result of this more elaborate structure, it becomes harder to approximate the Young's modulus. I have provided a suitable value of 0.16×10^9 Pa, just above a typical value for tough rubber.

A standard decaying exponential function, as shown in Figure (6.3), provides a great basis in modelling a tentacle, where the combination of external conditions generates the exaggerated whipping motion. Figure (6.3a) exemplifies the type of behaviour tentacles are expected to possess; the tight coiling at the end can be used to grapple under-water objects and similar to the previous sperm cell example, this whipping-like motion is efficient in generating movement.

(21) Tentacles move independently of the body they are attached to, whereas the sperm tail and body move and bend in unison.

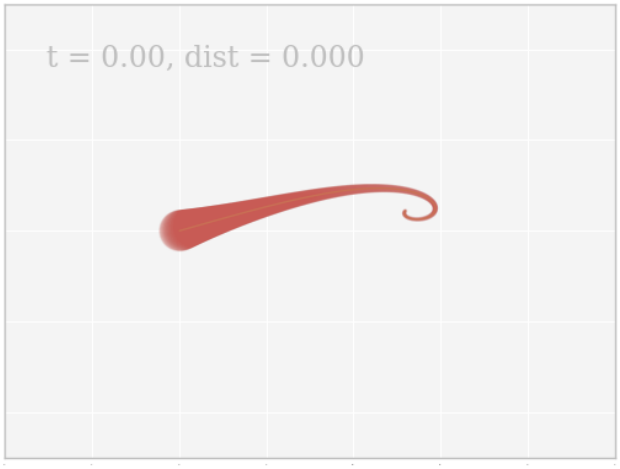

(a) **(b)**

Figure 6.3: **(a)** Numerical time solution of a rod with a significant exponential decaying thickness, representing the behaviour of octopus tentacles. $L = 2, m = 5, P = 1.3, \rho = 1.5, R(s) = 10e^{-2.8s}, \boldsymbol{\gamma} = [-0.3, 5, -5, 0.3], \boldsymbol{\delta} = [5, -2, 0.1, -0.5], E = 0.16 \times 10^9$. https://kapwi.ng/c/2EiUU53O. **(b)** Typical example of an octopus's tentacles. [27]

6.3.1 Variation in Curvature

Revisiting the derivation of the system, it is important to remember the assumptions made, ensuring these systems conform to what was assumed true. One such assumption made was that the curvature remains sufficiently small across its length. Up to this point, examples where the curvature grows exponentially large have not been encountered; however, in the example of tentacles, the tight coiling at the end of the arms begins to contradict this assumption.

Precisely, the assumption stated that the term $\left(\frac{\partial \theta}{\partial s}\right)^2$ vanishes (as discussed in Section (3.2)). However, in this particular case, the curvature $\frac{\partial \theta}{\partial s}$ can be calculated using the model, where it reaches a value over 20. Evidently, the square of this term cannot be simply ignored, but becomes the dominant term in the governing equation. This means that the general shape of Figure (6.3a) is not incorrect, but the inaccuracy of the solution is proportional to the curvature, becoming imprecise as the rod coils tighter.

6.4 Other Examples

As demonstrated by the preceding examples, applications of this model usually occur with varied thickness in biological instances. Whilst, as discussed earlier, Goyal, Perkins and Lee (2005) [5] analyse the instabilities of elastic rods and effect of supercoiling[(22)] in marine cables, cases of man-made examples do exist and present interesting research opportunities.

6.4.1 Auxetics

Auxetic materials are one example of this type of structure. All models thus far have been of non-auxetic materials, where the difference between the two materials arises from the sign of its Poisson ratio. Auxetic materials subjected to stretching longitudinally do not become thinner but the opposite: growing thicker in a perpendicular dimension (Comet, 2016) [28]. There are in fact naturally-occurring structures that have this type of behaviour, one example is silicate α-cristobalite (Grima et al., 2005) [29].

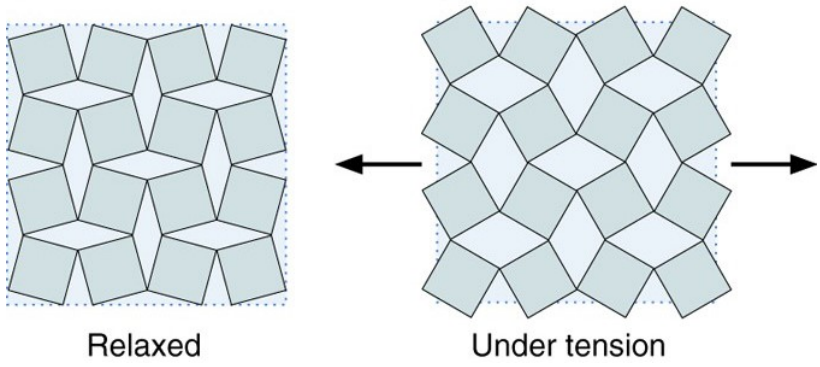

Figure 6.4: Typical behaviour of auxetic materials under an applied force. [30]

The dynamical changes in the internal structure of auxetic materials require very specific bending and twisting in order to create this defining deformation, which is why it is not possible to trivially incorporate into this model. The importance of twisting to this motion cannot be overstated, implying that a three-dimensional model must be used. Despite this, it is clear the internal structure should vary periodically, similar to the method by which the flexural rigidity and material density are varied.

(22) Supercoiling is the process by which lengths of rod excessively twist (coil), while becoming entangled. Usually associated with DNA.

DNA and flagella are two examples researchers commonly use in the Kirchhoff elastic rod model. Whilst DNA requires an element of twisting to function, flagella demonstrates a striking resemblance to the exponential whipping motion of elastic rods in this paper. As shown by Park et al. (2017) [31], the flagella can be modelled on a rotary motor to demonstrate an enforced whipping motion. Although their paper has observed the buckling instabilities, it also makes use of an equilibrium model and assumes a constant radius, which, as already shown, produces a significant shift in behaviour.

Section 7

Conclusions

On the mathematical modelling of the elastica theory, researchers often assume that the structure of elasticated rods and knots are uniform; this includes both the internal and external structure. In reality, this assumption can be valid for small deviations in structure, but restricts the freedom to accurately model rods with even a moderate change in profile. This idea is reinforced by the conclusions in Section (5.2), where significant changes in profiles in the exponential case can be seen. Again, looking at types of auxetic materials, ignoring any variation in internal structure completely disregards their defining behaviour. This exemplifies just how critical the inclusion of a varied bending stiffness and material density can be to the solution. Applications within engineering are particularly crucial, as variations, even to the degree of millimetres, can cause catastrophic damage to a structure.

7.1 Numerical Conclusions

Conclusions already made, have been based, generally, on visualisation. The change in behaviours in the rods are coherently communicated through the simulations, such that numerical evaluations only reaffirm the visual conclusions. I have used various types of numerical conclusions throughout the models in order to quantitatively support these conclusions.

By comparison, one would suspect that for the same conditions, *i.e.* only varying the radial function, a rod exhibiting this whipping motion oscillates at a greater amplitude than a rod exemplifying a waving behaviour. A quick, visual assessment supports this theory, yet by comparison of the antenna and tentacle examples, it is possible to measure the distance travelled by the end point of both rods, given the same periodicity. After a time $t = 1.50$,

the antenna (of length 6) travels a total distance of 18.270, whilst the tentacle (of length 2) only traces a curve of length 9.633; yet, comparatively measured as a proportion of length, the tentacle oscillates at a greater *relative* magnitude.

In Section (5.2), a comparison between the two types of motion and a uniform structured rod is given. Even though the conditions vary slightly[23] the magnitude of deviation is great. However, given the same conditions in both cases, it becomes apparent that the deviation of the sinusoidal example becomes negligible, further demonstrating the difference in dynamics between the two simulations. By measuring deviation as a proportion of total length, the sinusoid deviation rises to a maximum value of 0.053, whereas the exponentially decaying rod reaches a maximum value of 0.413. In both cases, this occurs at the end point of the rods; however, in general, it should not necessarily be assumed that the maximum deviation will always occur here and each instance should be investigated separately.

7.2 Limitations of the Model

One distinctly noticeable feature common in all of the rods is achirality. Similar to symmetry, it is the property that at some further point in time, the mirror image of the rod also exists. Relating to any example from our model, the mirror image of any single snapshot of the rod also occurs within the time loop. This is an inherent feature from the assumption that some (unstated) forces would satisfy our system. Looking beyond this project, it may be possible to state explicit forces, varied over time, to eliminate this constraint to the solution.

Whilst conditions like this increase the complexity of the system, it is still mathematically solvable. However, as noticed by Shan and Chen (2013) [32], the instability of thin elastic rods presents a problem for the existence for viable solutions. In particular, I notice that in the case of very thin rods, the solution does not converge, and interestingly, also for exponentially decaying rods of substantial length. This is the reason for using relatively short lengths in any exponential case, as well as dividing numerical conclusions by length for comparison.

Perhaps the biggest hindrance to the accuracy of solutions in the model was some of the assumptions made. To recall, the majority of these assumptions were made so that the system could be numerically solved and were entirely necessary to do so. However, it is possible that different methods and alternative assumptions could be beneficial to the model.

[23] As mentioned previously, this was intentional to highlight the defining behaviour of a sinusoidal rod.

7.3 Retrospective Approach

While it was stated that the governing differential equations in Section 2 were non-linear, it was assumed that the non-linear term vanishes. This made the system significantly easier to solve, but in particular cases provided approximations of the solution. As a result of limitations of the initial, given system[(24)], the non-linear terms have been appropriately ignored. However, applying the same numerical methods for solving ODEs, it is possible to discount this assumption all together and generate simulations of extreme curvatures.

Another assumption was that the expected solutions take a periodic form. If a different periodic function was applied, rather than a combination of sinusoidal functions in the Fourier series, a change in solutions could have been observed.

7.4 Future Research and Applications

Having already shown that overlapping solutions are not plausible as a result of contact mechanics, it is possible that the modelling of post-buckling behaviour can be included to show the effects of structural weakening, as researched by Almet et al. (2019) [33]. One might theorise that minimum points of a sinusoidal radial function are likely to display this type of buckling behaviour under tension. This may in fact be modelled by a variation in material density; however, the onset of buckling behaviour occurs over time, so it would not be trivial to incorporate into this model.

Mathematical modelling is a process by which a description of a dynamical system is produced using mathematical and physical theory. This branch of mathematics aims to simulate and reproduce real-world examples in near ideal conditions. In microscopic biology, future applications of models, similar to the one used in this paper, are seemingly limitless.

The primary purpose of bacterial flagellum is movement, but these appendages also react to disparities in chemical makeup and temperature (BiologyDictionary.net) [34]. By modelling the precise movement of bacterial flagella motors[(25)], it becomes possible to manipulate the movement and behaviour of bacterium. Furthermore, this can be used to target particular areas of the body, using bacteria as a vessel for drugs, or on the contrary, inhibit the movement of harmful bacteria, as discussed by Baker and Matzke (2019) in their article titled: 'Evolution or intelligent design? The story of the bacterial flagellar motor' [35].

[(24)] The initial, given system refers to the set of equations (3.9)-(3.11) where the non-linear terms did not appear.

[(25)] As discussed by Park et al. (2017) [31].

Similar theory was taken further by Zhang et al. (2009) [36], introducing the concept of an artificially controlled bacteria using electromagnetic fields, initially tested in water using a soft magnetic head.

From the Kirchhoff rod theory first introduced in 1859 to the present day, the growth and diversity of studies into the topic of elastica theory has allowed research to span a plethora of disciplines. In this paper, I proudly contribute to this ever-growing research domain by introducing variations in material structure. Proposing the idea of categorical solutions based on behaviour and real-world function helps to subdivide any future behaviours according to type of motion displayed.

Upon giving comparison to both common real-world examples and assumed uniform structures, my focus has been to coherently and justifiably communicate the consequential importance of including even a slight variation in structure.

Glossary

Appendages

> A section of an organism that protrudes from its body, having a unique and adapted function.

Bifurcation conditions

> Any small alteration to the input values can cause a significant topological change to the rod. As an example, the formation of loops in the rod cause instability.

Collocation scheme

> An algorithm for the numerical solution of ODEs by choosing a family of solution functions evaluating at numerous points in the domain. [37]

Critical buckling load

> The critical load at which the object subjected to a force suddenly deforms its profile.

Damped Newton method

> Used in conjunction to a collocation scheme, this is a method used to find roots of a real-valued function.

Flagella

> A whip-like appendage occurring on bacteria, that serves as an aid for movement and chemotaxis. [38]

Flexural modulus

> A measure of the material's resistance to bending when a force is applied orthogonal to the longest edge of the rod.

Poisson ratio

> The Poisson ratio measures the ratio of lateral strain to longitudinal strain. With typical values lying in the range of 0 to 0.5.

Serial homology

> The process of evolution by which various organs or appendages adapt to provide alternative functions.

Variational theorem

> A variational principle is a method, enabling a particular problem to be solved using the calculus of variations via optimisation.

Bibliography

[1] Kirchhoff, G. (1859). 'Ueber das Gleichgewicht und die Bewegung eines unendlich dünnen elastischen Stabes'. *Journal für die reine und angewandte Mathematik 1859*, vol. 56, DOI: 10.1515/crll.1859.56.285.

[2] Clebsch, A. (1862). 'Theorie der Elasticitat Fester Korper'.

[3] Matsutani, S. (2010). 'Euler's elastica and beyond'. *Journal of Geometry and Symmetry in Physics*, vol. 17.

[4] Dill, E.H., (1992). 'Kirchhoff's theory of rods'. *Arch. Hist. Exact Sci*, vol. 44, DOI: 10.1007/BF0037968.

[5] Goyal, S., Perkins, N.C. and Lee, C.L. (2005). 'Nonlinear dynamics and loop formation in Kirchhoff rods with implications to the mechanics of DNA and cables'. *Journal of Computational Physics*, vol. 209, DOI: 10.1016/j.jcp.2005.03.027.

[6] Dias, M.A., Audoly, B. (2015). '"Wunderlich, Meet Kirchhoff": A General and Unified Description of Elastic Ribbons and Thin Rods'. *Journal of Elasticity*, vol. 119, DOI: 10.1007/s10659-014-9487-0.

[7] Silverman, M. and Farrah, J. (2018). 'Bending of a Tapered Rod: Modern Application and Experimental Test of Elastica Theory'. *World Journal of Mechanics*, vol. 8, DOI: 10.4236/wjm.2018.87022.

[8] Weiss, H. (2002). 'Dynamics of Geometrically Nonlinear Rods: II. Numerical Methods and Computational Examples'. *Nonlinear Dynamics*, vol. 30, DOI: 10.1023/A:1021257410404.

[9] Prior, C. (2020). 'Mathematical Biology Notes'. *University of Durham*, Chapter 6: Elastic Tubes and Biopolymers.

[10] Antman, S. (1995). 'Nonlinear Problems of Elasticity'. *Applied Mathematical Sciences*, vol. 107, DOI: 10.1007/978-1-4757-4147-6.

[11] Fourier, J. (1822). 'Théorie analytique de la chaleur'.

[12] Xavier, Ademir L., J. (2014). 'Static Kirchhoff Rods under the Action of External Forces: Integration via Runge-Kutta Method'. *Journal of Computational Methods in Physics*, vol. 2014, DOI: 10.1155/2014/650365.

[13] Goriely, A., Nizette, M. and Tabor, M. (2001). 'On the Dynamics of Elastic Strips'. *Journal of Nonlinear Science*, vol. 11, DOI: 10.1007/s003320010009.

[14] The SciPy community. https://docs.scipy.org/doc/scipy/reference/generated/scipy.integrate.odeint.html (accessed March 25, 2021).

[15] Wikiversity contributors. 'Adams-Bashforth and Adams-Moulton methods'. Wikiversity, https://en.wikiversity.org/w/index.php?title=Adams-Bashforth_and_Adams-Moulton_methods&oldid=2209802 (accessed April 13, 2021).

[16] The SciPy community. https://docs.scipy.org/doc/scipy/reference/generated/scipy.integrate.solve_bvp.html (accessed March 25, 2021).

[17] Engineering ToolBox. (2012). 'Euler's Column Formula'. https://www.engineeringtoolbox.com/euler-column-formula-d_1813.html (accessed April 14, 2021).

[18] Helmenstine, A. 'What Is Young's Modulus?'. *ThoughtCo*, https://www.thoughtco.com/youngs-modulus-4176297 (accessed April 25, 2021).

[19] (2002). 'Crustaceamorpha: Appendages'. *University of California Museum of Paleontology*. https://ucmp.berkeley.edu/arthropoda/crustacea/appendages.html. (accessed April 10, 2021).

[20] Boxshall, G., Jaume, D. (2013). 'Antennules and Antennae in Crustacean'. *Functional Morphology and Diversity*, DOI: 10.1093-/acprof:osobl/9780195398038.003.0007.

[21] Vickery, R., Hollowell, K. and Hughes, M. (2012). 'Why have long antennae? Exploring the function of antennal contact in snapping shrimp', *Marine and Freshwater Behaviour and Physiology*, vol. 45, DOI: 10.1080/10236244.2012.699644.

[22] Guerin, L. Image licensed by CK-12 Foundation. https://www.ck12.org/biology/crustaceans/lesson/crustaceans-advanced-bio-adv/

[23] Loudon, C. (2005). 'Flexural Stiffness of Insect Antennae'. *American Entomologist*, vol. 51, DOI: 10.1093/ae/51.1.48.

[24] MicroscopeMaster. 'Adaptations of Sperm Cells'. https://www.microscopemaster.com/sperm-cells.html (accessed April 15, 2021).

[25] Image designed by brgfx/Freepik. https://www.freepik.com/free-vector/sperm-cell-structure_2451326.htm

[26] Hall, D. 'Cephalopods'. *Smithsonian Institute*. https://ocean.si.edu/ocean-life/invertebrates/cephalopods (accessed April 19, 2021).

[27] ShutterStock. https://www.shutterstock.com/image-photo/tentacles-octopus-isolated-on-white-background-717916195

[28] Comet, C. (2016). 'Auxetics'. *ELISAVA – Barcelona School of Design and Engineering*, http://materiability.com/portfolio/auxetics/ (accessed April 20, 2021).

[29] Grima, J., Gatt, R., Alderson, A. and Evans, K. (2005). 'On the origin of auxetic behaviour in the silicate -cristobalite'. *Journal of Materials Chemistry*, vol. 15, DOI: 10.1039/B508098C.

[30] Dagdelen, J., Montoya, J., de Jong, M. and Persson, K. (2017). 'Computational prediction of new auxetic materials'. *Nature Communications*, vol. 8, DOI: 10.1038/s41467-017-00399-6.

[31] Park, Y., Kim, Y., Ko, W. and Lim, S. (2017). 'Instabilities of a rotating helical rod in a viscous fluid'. *Physical Review*, vol. 95, DOI:10.1103/PhysRevE.95.022410.

[32] Shan, W. and Chen, Z. (2013). 'Mechanical Instability of Thin Elastic Rods'. *Journal of Postdoctoral Research*, vol. 1, DOI: 10.14304/SURYA.JPR.V1N2.1.

[33] Almet, A., Byrne, H., Maini, P. and Moulton, D. (2019). 'Post-buckling behaviour of a growing elastic rod'. Journal of Mathematical Biology, vol. 78, DOI:10.1007/s00285-018-1292-0.

[34] Biologydictionary.net Editors. (2017). 'Flagellum' *Biology Dictionary, Biologydictionary.net*, https://biologydictionary.net/flagellum/.

[35] Baker, M. and Matzke, N. (2019). 'Evolution or intelligent design? The story of the bacterial flagellar motor'. *ABC Science*, https://www.abc.net.au/news/science/2019-11-07/evolution-supported-by-bacterial-flagellar-motor/11635276

[36] Zhang, L., Abbott, J., Dong, L., Kratochvil, B., Zhang, H., Peyer, K., and Nelson, B. (2009). 'Micromanipulation Using Artificial Bacterial Flagella'. *IEEE/RSJ International Conference on Intelligent Robots and Systems*, DOI: 10.1109/IROS.2009.5354314.

[37] 'Collocation method'. *Encyclopedia of Mathematics*. http://encyclopediaofmath.org/index.php?title=Collocation_method&oldid=46399 (accessed April 19, 2021).

[38] Haiko, J. and Westerlund-Wikström, B. (2013). 'The role of the bacterial flagellum in adhesion and virulence'. *Biology (Basel)*, DOI:10.3390/biology2041242.

[39] Huynen, A., Detournay, E. and Denoël, V. (2016). 'Eulerian formulation of elastic rods'. *Proceedings of the Royal Society A: Mathematical, Physical and Engineering Science*, vol. 472, DOI: 10.1098/rspa.2015.0547.

[40] Kapwing website. https://www.kapwing.com (accessed April 29, 2021).

[41] Wolfram Alpha website. https://www.wolframalpha.com/ (accessed April 29, 2021).

Durham University

Section A

Appendix A

A.1 Python Code using odeint

```
# Module imports

import math, sympy, numpy as np, matplotlib.pyplot as plt, sys, os,
    datetime
from scipy import integrate
from scipy.integrate import odeint
from pylab import *
from matplotlib.collections import LineCollection
os.environ["IMAGEIO_FFMPEG_EXE"] = "/usr/bin/ffmpeg"
import moviepy.video.io.ImageSequenceClip

# Plot customisation

plt.style.use('seaborn-dark')
plt.rcParams['xtick.labelsize'] = 0
plt.rcParams['ytick.labelsize'] = 0
plt.rcParams['axes.prop_cycle'] = plt.cycler(color=["#0c2c6b", "#
    f4f4f4", "0.7"])
plt.rcParams['axes.facecolor'] = '#f4f4f4'
plt.rcParams['axes.grid'] = True
plt.rcParams['axes.edgecolor'] = '#bfbfbf'
plt.rcParams['axes.linewidth'] = 1
plt.rcParams['grid.color'] = '#ffffff'
plt.rcParams['font.family'] = 'serif'

 # Definitions
```

```
25
26  # N: No. of iterations for the solution, for individual times.
27  # L: Length of the rod.
28  # r0: Starting position (independent of t) [.,.]
29  # m: No. of modes.
30  # P: Period of repetition.
31  # I: Area moment of inertia.
32  # rho: Material Density (can be varied in s)
33  # R: Radial functions defining variation in thickness.
34  # B: Bending Stiffness: (pi*E*R**4)/4. Given some E: Young's modulus
        .
35  # trange: Range of time.
36  # gamvec, delvec: Initial boundary conditions.
37  # Bdash: Explicit derivative of B (defaults to zero).
38
39  def imgsoln(N, L, r0, m, P, rho, R, B, trange, gamvec, delvec, Bdash
        = 0):
40      co = -1
41      tno = 368 # Number of time steps from 0 to trange.
42      for t in np.linspace(0, trange, tno):
43          co += 1
44          cosint, sinint = [], []
45          if (type(B) is list): # B entered as a polynomial
46              q = sympy.Symbol('q')
47              poly = sum(c*q**i for i, c in enumerate(B))
48              Bdash = sympy.diff(poly)
49          for i in range(1,N+1):
50              b = i*L/N
51              s = np.linspace(0, b, 40)
52
53              if (type(B) is list):
54                  Bfunc1 = poly.evalf(subs={q:b})
55                  Bdash1 = Bdash.evalf(subs={q:b})
56              elif callable(B) and Bdash != 0:
57                  Bfunc1 = B(b)
58                  Bdash1 = Bdash(b)
59              else:
60                  print('B or Bdash given incorrect input.')
61                  sys.exit()
62
63              I = (np.pi*(R(b))**4)/4 # Area moment of inertia defined
        from the radial function R.
64              coefs = [Bfunc1/(m**2*P**2*rho), Bdash1/(m**2*P**2*rho),
```

```
    I, 0, -1]
65          def vectorf(w, s): # Convert fourth-order differential
    equation into four first-order ODEs.
66              x1, x2, x3, x4 = w
67              f = [x2, x3, x4, (x1-coefs[2]*x3-coefs[1]*x4)/coefs
    [0]]
68              return f
69
70          sol1m = odeint(vectorf, gamvec, s)
71          # Solved using odeint.
72          sol2m = odeint(vectorf, delvec, s)
73          x1 = sol1m[:,0] # b1m
74          x3 = sol1m[:,2] # d2b1m/ds2
75          y1 = sol2m[:,0] # b2m
76          y3 = sol2m[:,2] # d2b2m/ds2
77
78          a1m = (-1/m**2*P**2*rho)*np.array(x3)
79          a2m = (-1/m**2*P**2*rho)*np.array(y3)
80          theta = a1m*np.cos(m*P*t)+a2m*np.sin(m*P*t)
81          # Introduction of t depedence.
82          integrand = [np.cos(theta), np.sin(theta), 0]
83          cosint.append(integrate.simps(integrand[0],s))
84          # Numerical integration using Simpson's rule.
85          sinint.append(integrate.simps(integrand[1],s))
86
87      x, y = np.array(cosint), np.array(sinint)
88
89      # Visual representation of a varied thickness.
90
91      lwidths = []
92      for p in np.linspace(0,L,len(x)):
93          lwidths.append(50*R(p))
94      fig, axes = plt.subplots()
95
96      axes.scatter(x+r0[0],y+r0[1], s=lwidths, alpha=0.05)
97      axes.plot(x+r0[0],y+r0[1],"#4e596e",linewidth=1)
98      axes.set_xlim(-1+r0[0], L+0.5+r0[0])
99      axes.set_ylim(-0.5+r0[1]-L, L+0.5+r0[1])
100
101     plt.suptitle('t = %.2f' % np.round(t,2), x=0.24, y=0.81, size
    =17, color='#bfbfbf')
102     # plt.show()
103     fig.savefig(("{1}/oscplot_{0}.png").format(int(co),file))
```

```
        plt.rcParams.update({'figure.max_open_warning': 0})

 # Test cases.

x = [600, 2.1, [3,5], 5, 1, 1.5, lambda x:3*(np.sin(9*x)+1.3), lambda
     x:(np.pi*1.2e4/4)*(3*(np.sin(9*x)+1.3))**4, 5, [1,1,1,1],
    [1,1,1,1], lambda x:(np.pi*1.2e2/4)*(2916*np.cos(9*x)*(np.sin(9*x
    )+1.3)**3)]

file = str(datetime.datetime.now().replace(microsecond=0)).replace("
    ","-").replace(":",".")
os.makedirs(file)
imgsoln(*x)

image_files = [file+'/'+img for img in os.listdir(file) if img.
    endswith(".png")]
clip = moviepy.video.io.ImageSequenceClip.ImageSequenceClip(
    image_files, fps=13)
clip.write_gif('{0}.gif'.format(file))
```

A.2 Python Code Snippet for `solve_bvp`

```
def vectorf(s, w): # Convert fourth-order differential equation into
    four first-order ODEs.
    f = np.vstack((w[1], w[2], w[3], (w[0]-coefs[2]*w[2]-coefs[1]*w
    [3])/coefs[0]))
    return f
def bc(ya, yb):
    return  np.array([ya[0]-0.5, yb[0]-0.5, ya[1], yb[1]+2])
y_a = np.ones((4, s.size))
y_b = np.ones((4, s.size))

sol1m = solve_bvp(vectorf, bc, s, y_a) # Solved using solve_bvp.
sol2m = solve_bvp(vectorf, bc, s, y_b)
```